Remarks on Two-Higgs-Doublet Models

Jack Gunion

U.C. Davis

KITP2016 Experimental Challenges, April 19, 2016

Papers/collaborators:

1. Constraints on and future prospects for Two-Higgs-Doublet Models in light of the LHC Higgs signal: Dumont, Gunion, Jiang, Kraml, arXiv:1405.3584.

2. Light Higgs bosons in Two-Higgs-Doublet Models: Bernon, Gunion, Jiang, Kraml, arXiv:1412.3385.

3. Scrutinizing the alignment limit in two-Higgs-doublet models: Bernon, Gunion, Haber, Jiang, Kraml, arXiv:1507.00933 ($h125$), arXiv:1511.03682 ($H125$). Plots in these papers are for $C_V \geq 0.99$.

Experimental situation for heavy Higgs bosons decaying to lighter stuff was summarized in Klute's talk.

- The fairly SM-like nature of the 125 GeV state provides important constraints, but there is still a lot of freeedom.
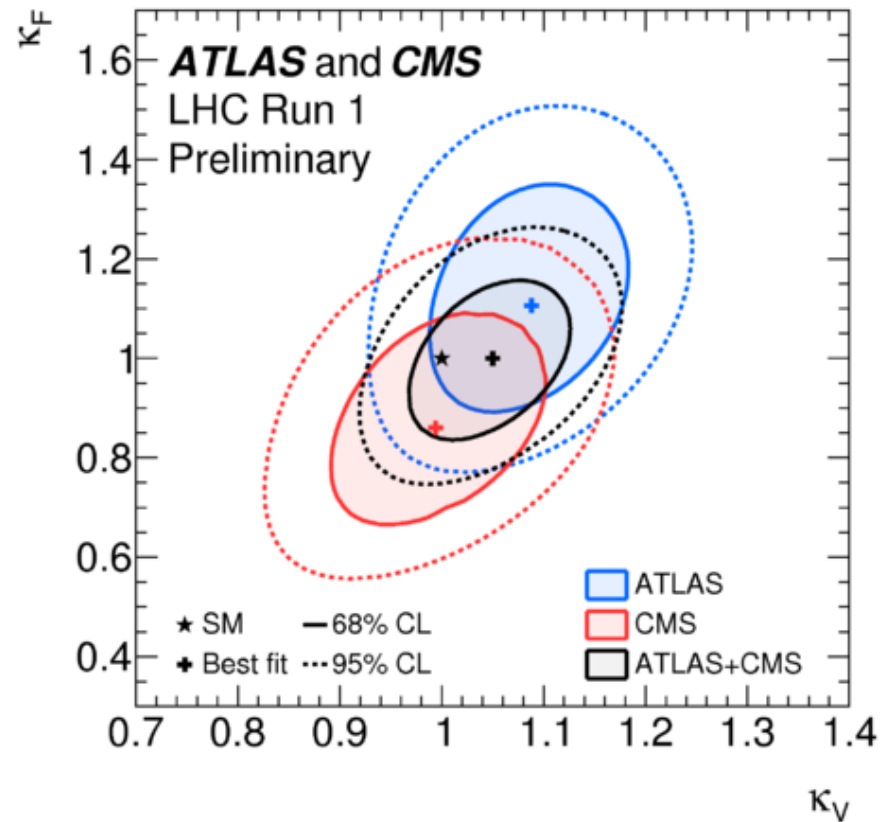

Figure 1: κ_F versus κ_V for the combination of ATLAS and CMS and for the global fit of all channels. Also shown are the contours obtained for each experiment. From ATLAS-CONF-2015-044.

- There can be unseen, U, but not truly invisible, decays of the SM-like Higgs.

When C_U, C_D are free, $C_V \leq 1$ and $\Delta C_\gamma = \Delta C_g = 0$, $\mathcal{B}_U < 0.22$ at 95% CL.

- If the 125 GeV Higgs is very SM-like, i.e. the alignment limit, there are still many opportunities even if the only new particles are Higgs bosons. Ignoring the 750 GeV state, increasing limits on new physics suggests that one should take seriously this possibility.

    - we should consider limits of multi-Higgs models in which one of the Higgs bosons is really very SM-like;
    - given the current data set, heavier or lighter Higgs bosons can have escaped detection due to inadequate cross section;
    - lighter Higgs bosons could even be present in the decays of the 125 GeV state so long as the corresponding branching ratio is not so large as to violate the $\mathcal{B}_U$ limits above.

    2HDM models are the simplest prototypes for these possibilities.

- Of course, purely Higgs sector new physics has severe hierarchy/naturalness problems unless placed in the context of warped extra dimensions (e.g. RS). In the RS context, you can have any Higgs structure you like — the warping takes care of hierarchy.

Returning to $h125$ decays to lighter Higgs, of particular interest in the 2HDM are $h \to AA$ or $H \to AA, hh$. For acceptable $h125$ or $H125$ fits, respectively, must suppress the couplings if these are kinematically allowed. This can be achieved with some level of parameter fine-tuning.

Meaningful limits are only currently available for $m_A \lesssim 20$ GeV. Of those shown by Klute, only HIG-14-022 and HIG-14-019 give a meaningful constraint when $m_A > 2m_\tau$.
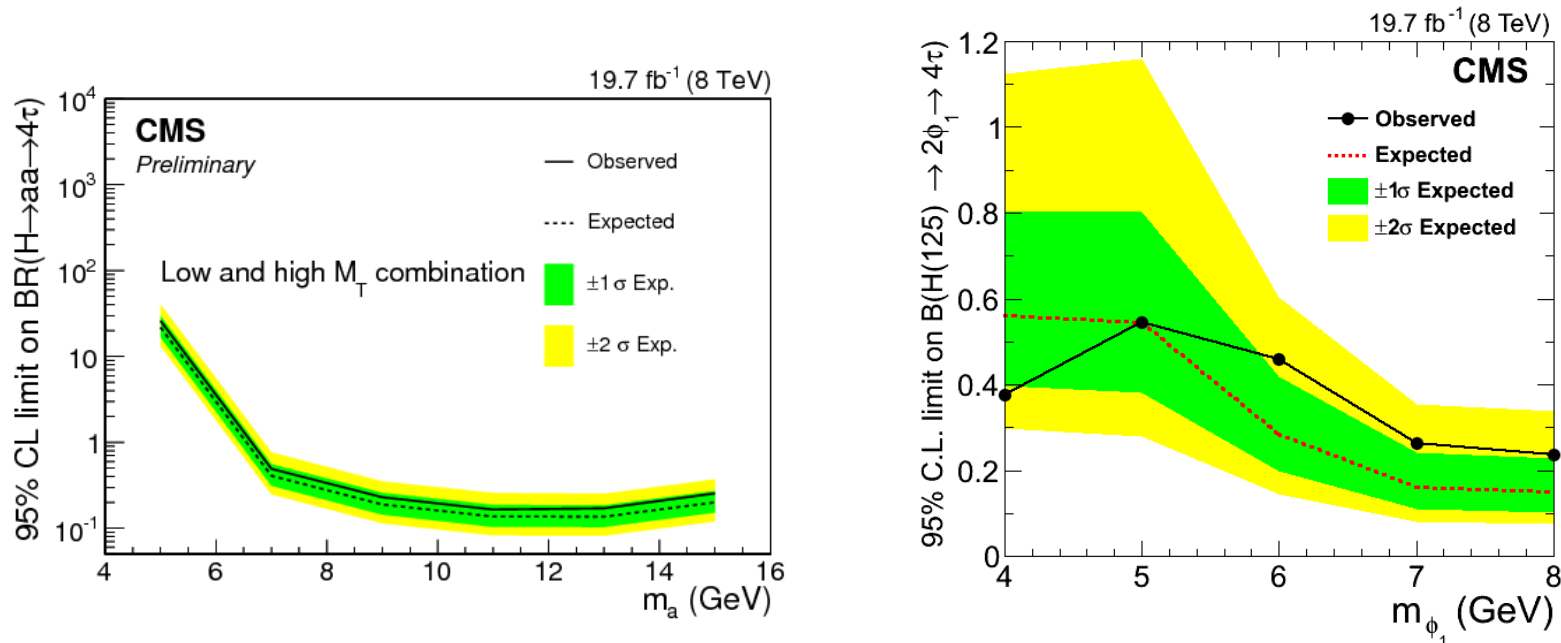

Figure 2: Limits on $\mathcal{B}(h125 \to aa \to 4\tau)$ from CMS analyses HIG-14-022 and HIG-14-019, respectively.

- Basic picture

2HDMfit (typeI) m_h=125.5±2.5 GeV
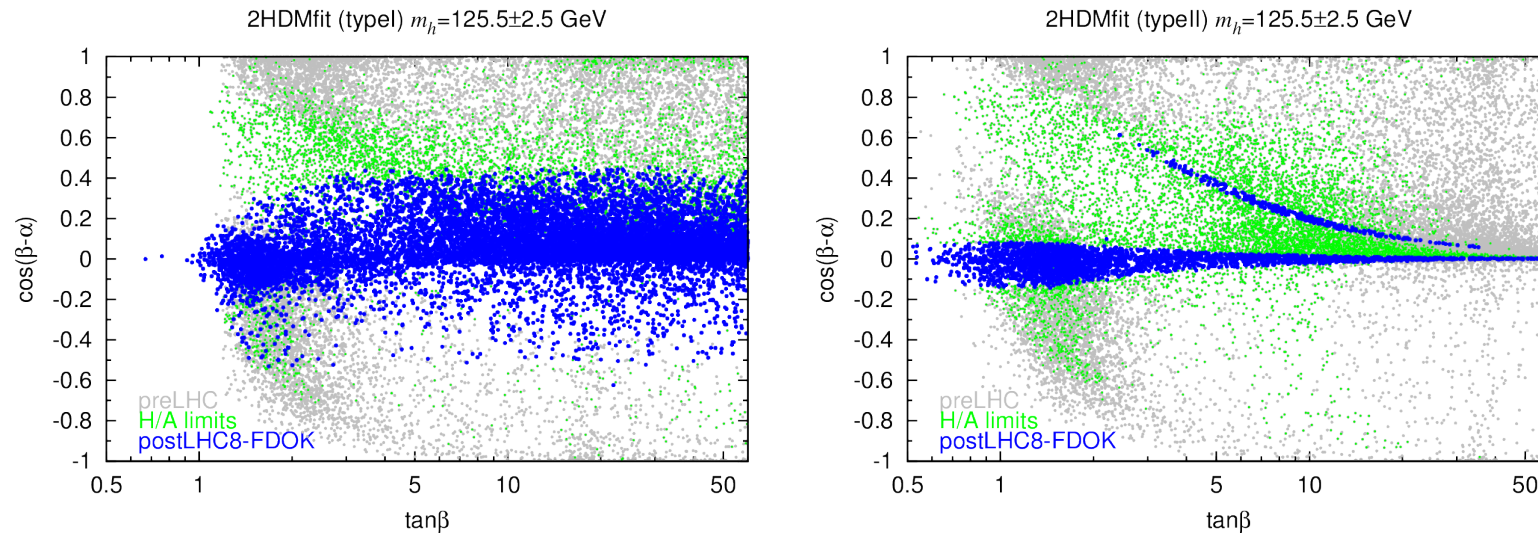
2HDMfit (typeII) m_h=125.5±2.5 GeV

Figure 3: Constraints in the $\cos(\beta - \alpha)$ versus $\tan\beta$ plane for $m_h \sim 125.5$ GeV. Grey points satisfy preLHC constraints, while green points satisfy in addition the pre-May-2014 LHC limits on H and A production. Blue points fall in addition within the 7+8 TeV 95% CL ellipses in the $[\mu(\mathrm{ggF} + \mathrm{ttH}), \mu(\mathrm{VBF} + \mathrm{VH})]$ plane for each of the final states considered, $Y = \gamma\gamma, ZZ, WW, b\bar{b}, \tau\tau$. From paper #1.

The SM limit is $\cos(\beta - \alpha) \to 0$. For Type II there is a main branch that is very SM-like, but also an alternative branch that is quite different. This is a branch

having $C_D^h \sim -1$. The future LHC run can eliminate or confirm this branch. (see, in particular, arXiv:1403.4736, Ferreira, Gunion, Haber, Santos.) (NB: $C_U^h \sim -1$ is ruled out at $> 5\sigma$.)

In the alignment limit and after including data not included above (see below), the extent of this "wrong-sign" branch is considerably restricted.

- What masses are possible for the heavy H and the A?

The situation is evolving rapidly as new constraints from Run1 are added and after latest $b \to s\gamma$ constraint of $m_{H^\pm} > 480$ GeV is included for Type II. Of particular importance: the 25 GeV $< m_A < 80$ GeV CMS limits from $b\bar{b}\phi$ with $\phi \to \tau\tau$ and the LEP limits on $b\bar{b}\phi$.
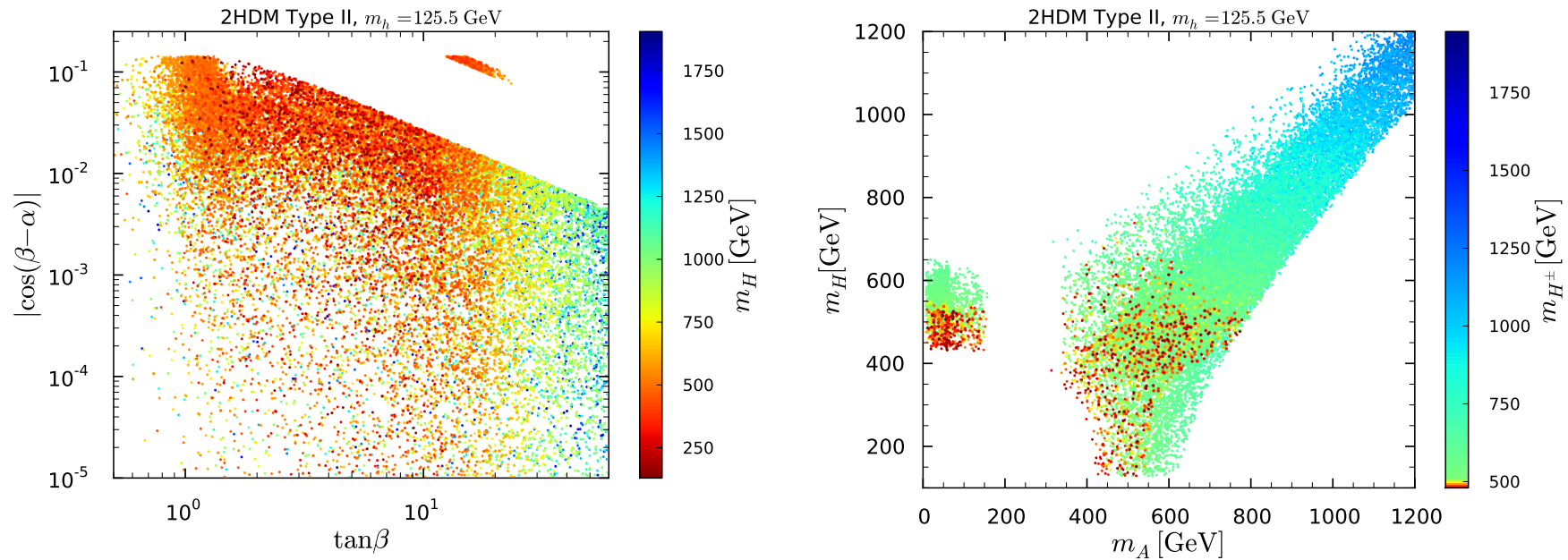
Figure 4: Constraints in the $\cos(\beta - \alpha)$ vs $\tan\beta$ and the m_H vs m_A plane for $m_h \sim 125.5$ GeV in Type II. Coloring in $m_{H\pm}$ from high to low. Plot includes recent $b \to s\gamma$ constraint of $m_{H\pm} > 480$ GeV and limits on bbA with $A \to \tau\tau$ for 25 GeV $< m_A < 80$ GeV, as well as constraints on $e^+e^- \to b\bar{b}A$.

From CMS-HIG-14-033, arXiv:1511.03610 we eliminate nearly all the Type II points with $m_A > 25$ GeV that have $C_D^h < 0$ (opposite sign to normal but same magnitude). The $m_A < 25$ GeV wrong sign points are eliminated by the DELPHI LEP limit (both Z-pole data and continuum data). All that is left of the wrong sign points are those with $m_A > 25$ GeV and $\tan\beta \geq 10$.

Note: These constraints apply equally to the (light) h of the Type II $H125$ scenario in the alignment limit where the $h b \bar{b}$ coupling is also $\simeq \tan \beta$.

- What channels could be of interest in the alignment limit.

  1. should not see ZZ and WW decays of the H since the h saturates those couplings.
     Nor should you see $A \to Zh$. Excesses in these searches are thus particularly important.
     But, of course, the alignment limit may not be exact, or there may be higher Higgs representations present.
  2. In $h125$ scenario should (eventually) see $H \to ZA$ if m_A is small enough — nothing so far (Klute).
  3. $H \to hh$ is certainly a possibility if $m_H > 250$ GeV, but this channel is hard — nothing so far (Klute), and large cross section is not guaranteed.
  4. In both Type I and Type II, $\sigma(gg \to A)$ have lower bounds. e.g. at $m_A = 1.2$ TeV, $\sigma(gg \to A) > 10^{-6}$ pb, 10^{-3} pb for Type I, Type II. — Obviously, Type II will be easier to eventually explore fully or eliminate.
  5. In Type II, $gg \to A$ with $A \to \tau\tau$ cannot have arbitrarily small cross section — for $m_A \leq 1$ TeV, $\sigma > 3 \times 10^{-3}$ fb (not wonderful, but something). Similar statement for H.
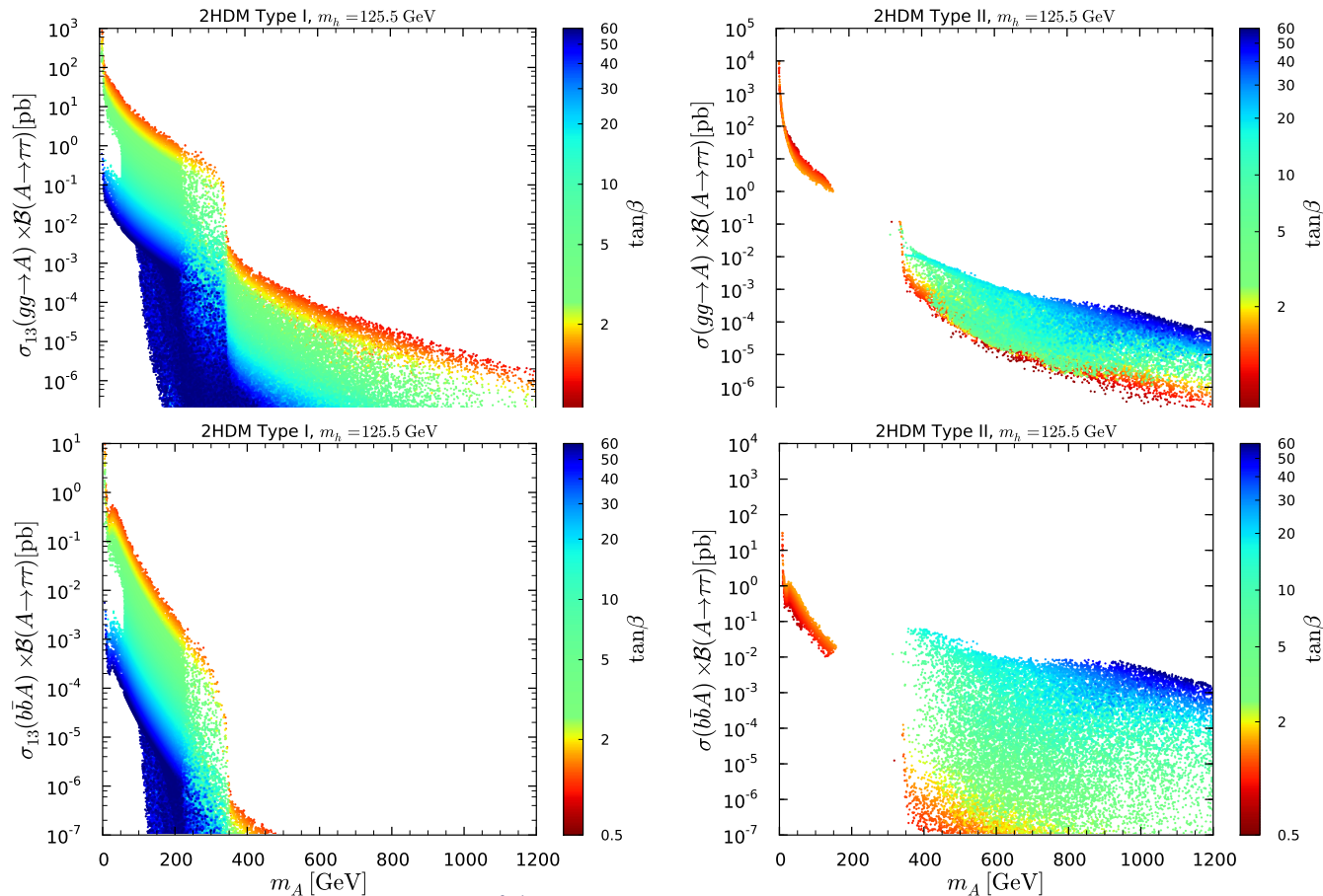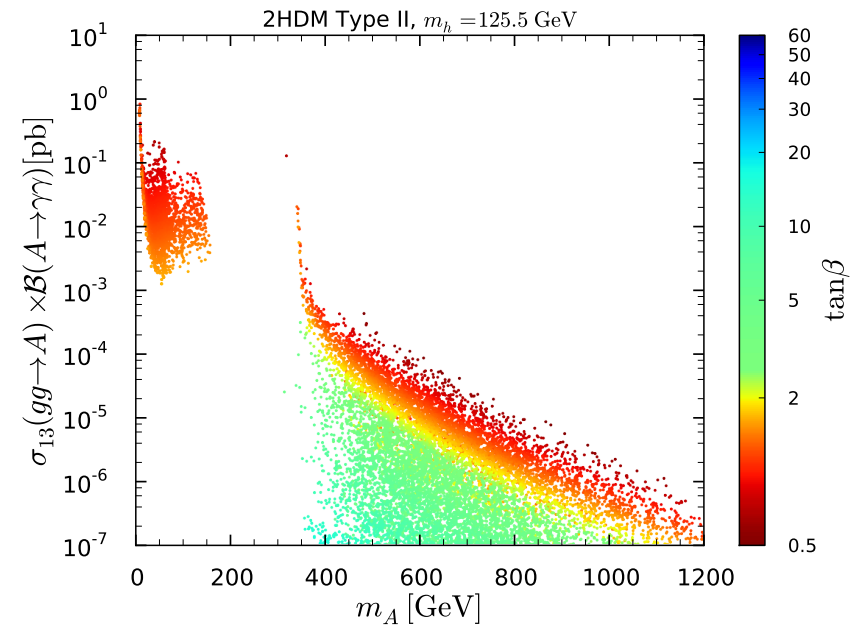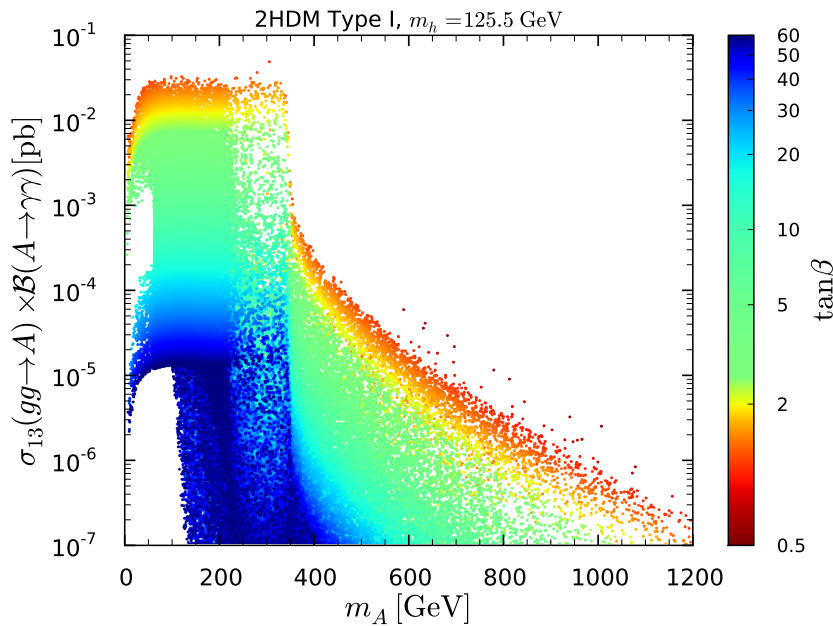
Figure 5: 2HDM points agreeing at 95% C.L. with precision Higgs data as well as B physics, ... Coloring in $\tan\beta$ from low to high.

- The only other potentially interesting channel for a light A is the $\gamma\gamma$ final state.

2HDM Type I, $m_h = 125.5$ GeV · 2HDM Type II, $m_h = 125.5$ GeV

Cross sections for Type II are really quite large at low m_A. (NB: the high $\tan\beta$ values in Type II were eliminated at low m_A by the bbA with $A \to \tau\tau$ CMS analysis and/or the LEP $b\bar{b}A$ limits so that we obtain a rather definitive cross section prediction.)

In Type I the cross section is also not so small if $\tan\beta$ is small, but is predicted to be very small at high $\tan\beta$.

At 750 GeV, $\gamma\gamma$ cross sections are of order a $few \times 10^{-2}$ fb, a factor 100 too small for claimed signal. Similar story for H. See also http://arxiv.org/abs/1512.07616

(Stefania and collaborators).

- A note on the wrong sign points.

The wrong-sign points are associated with a non-decoupling heavy charged Higgs loop contribution to the $h\gamma\gamma$ coupling leading to $C_\gamma^h \lesssim 0.96$ while $C_g^h \sim 1.07$ because top and bottom loop contributions to the hgg coupling add. (See also Ferreira *et al.*, arXiv:1403.4736.)
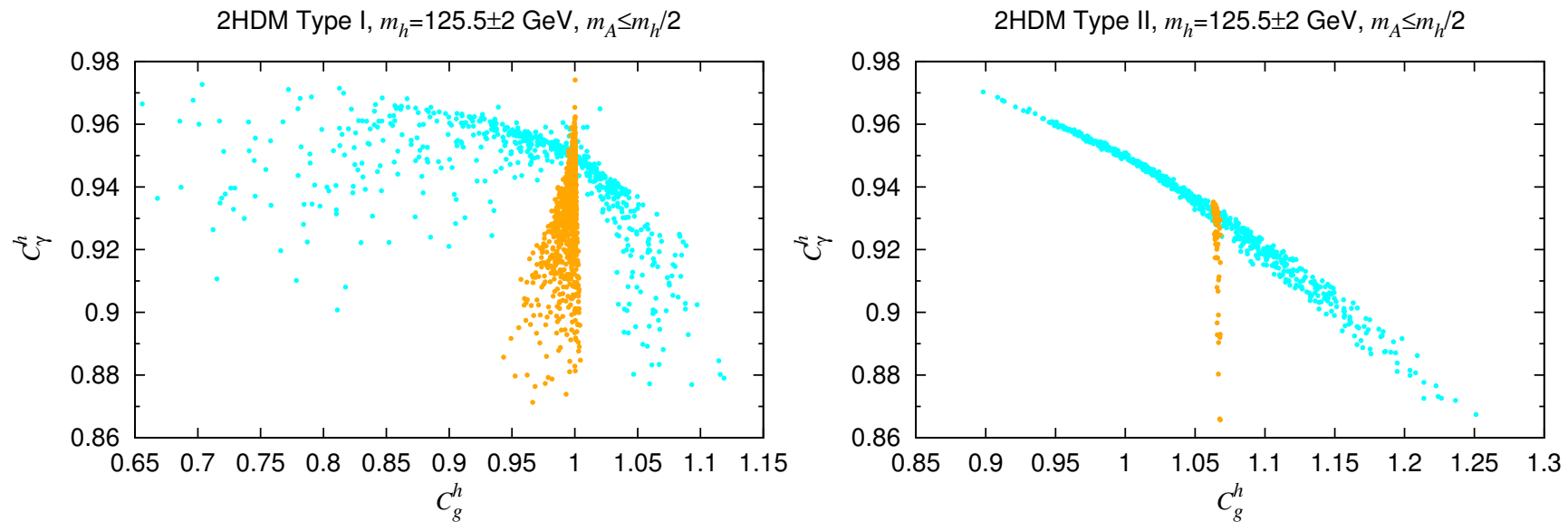

Figure 6: From paper #2. Orange points have $C_D \sim -1$.

Above, we plot C_g vs.C_γ, the hgg and $h\gamma\gamma$ couplings relative to the SM values. Can these deviations be measured? LHC, *but not ILC* will measure C_γ sufficiently

to discriminate from SM for Type II, and most Type I points. ILC and LHC reach similar C_g accuracies (2% vs. 3%) ultimately. But, C_g is useful only when correlated with C_γ.

<div style="border:1px solid; background:#ffffcc; display:inline-block; padding:4px;">

$H125$ case

</div>

Some basics:

- Here, the h is guaranteed to be light, but the A need not be and, in fact, cannot be light in the case of Type II because of STU constraints given $m_{H^\pm} > 480 \text{ GeV}$.

- The LHC limits on $A \to Zh$ have significant impact since the AhZ coupling is maximal in the $H125$ scenario.

- Recent LHC ATLAS and CMS limits on the $\tau\tau$ final state cut away a bunch of points that would apriori be allowed before including such limits.

In particular, you will see some cross section plots vs. m_h for Type II where constraints are strong for $m_h < 80 \text{ GeV}$ and for $m_h > 90 \text{ GeV}$ but much larger cross sections are possible for $m_h \in [80, 90] \text{ GeV}$. This Z-peak region is one that ATLAS and CMS must work on even though it is clearly hard.
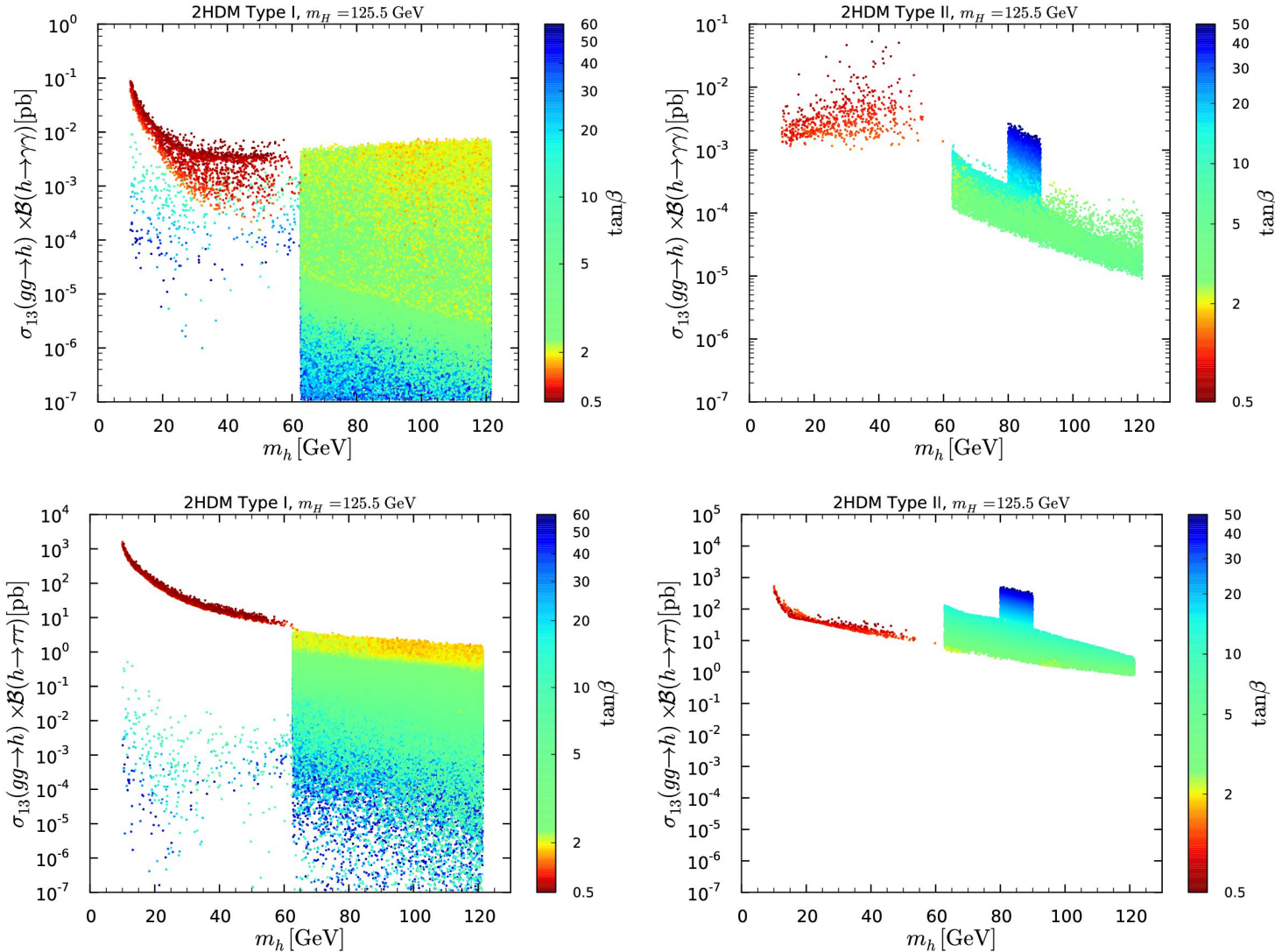
Figure 7: $\sigma(gg \to h \to Y)$ as functions of m_h for $Y = \gamma\gamma$ (upper panels) and $Y = \tau\tau$ (lower panels). Points are colored from high to low $\tan\beta$.

In the above plots, note the very well defined and large cross section for $gg \to h \to \tau\tau$ in the case of Type II. Type I $gg \to h$ cross sections get killed by large $\tan\beta$.
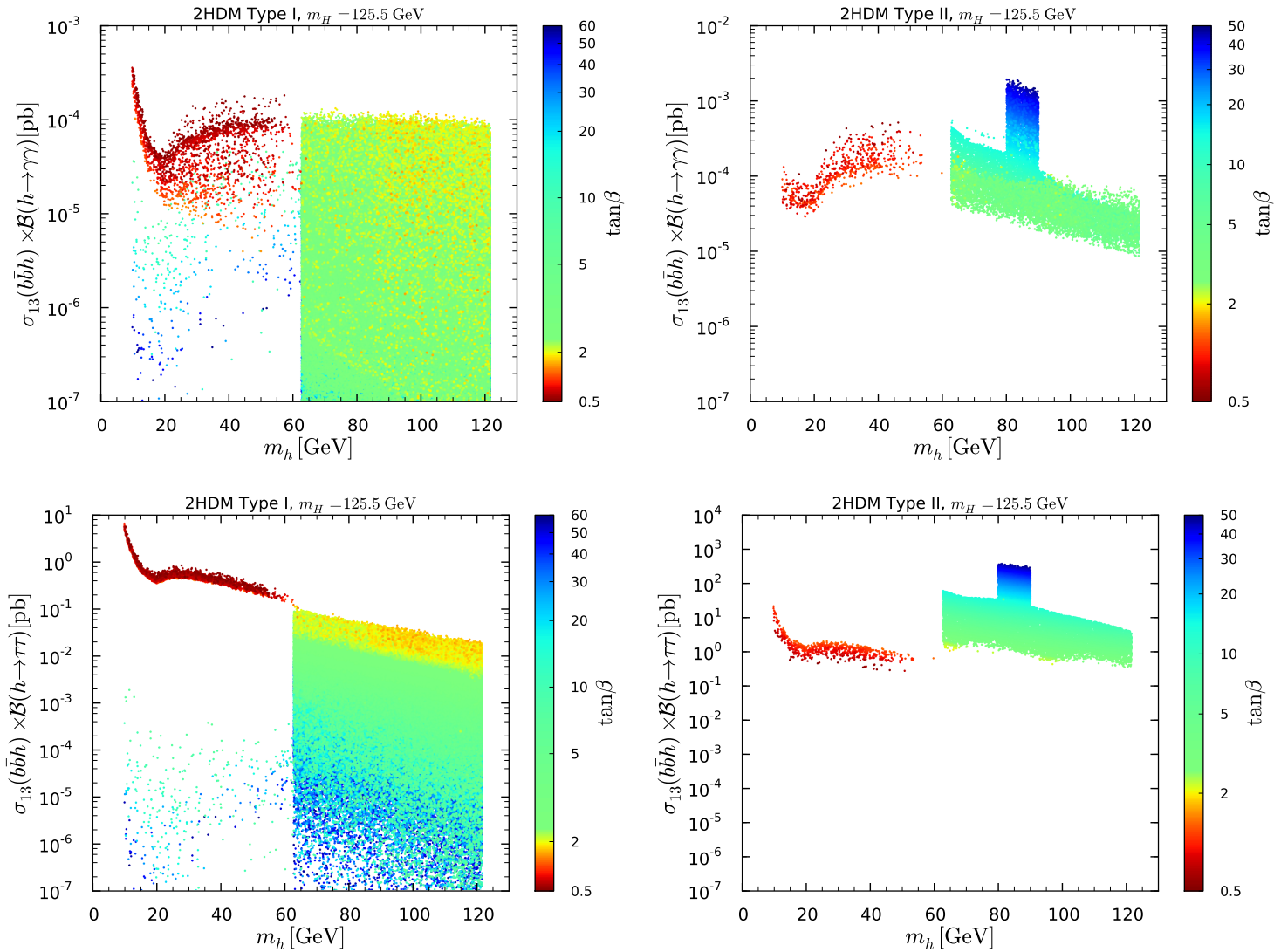
Figure 8: $\sigma(bbh) \times \mathcal{B}(h \to Y)$ as functions of m_h for $Y = \gamma\gamma$ (upper panels) and $Y = \tau\tau$ (lower panels). Points are colored from high to low $\tan\beta$.

The bbh cross sections are mostly somewhat lower than $gg \to h$.
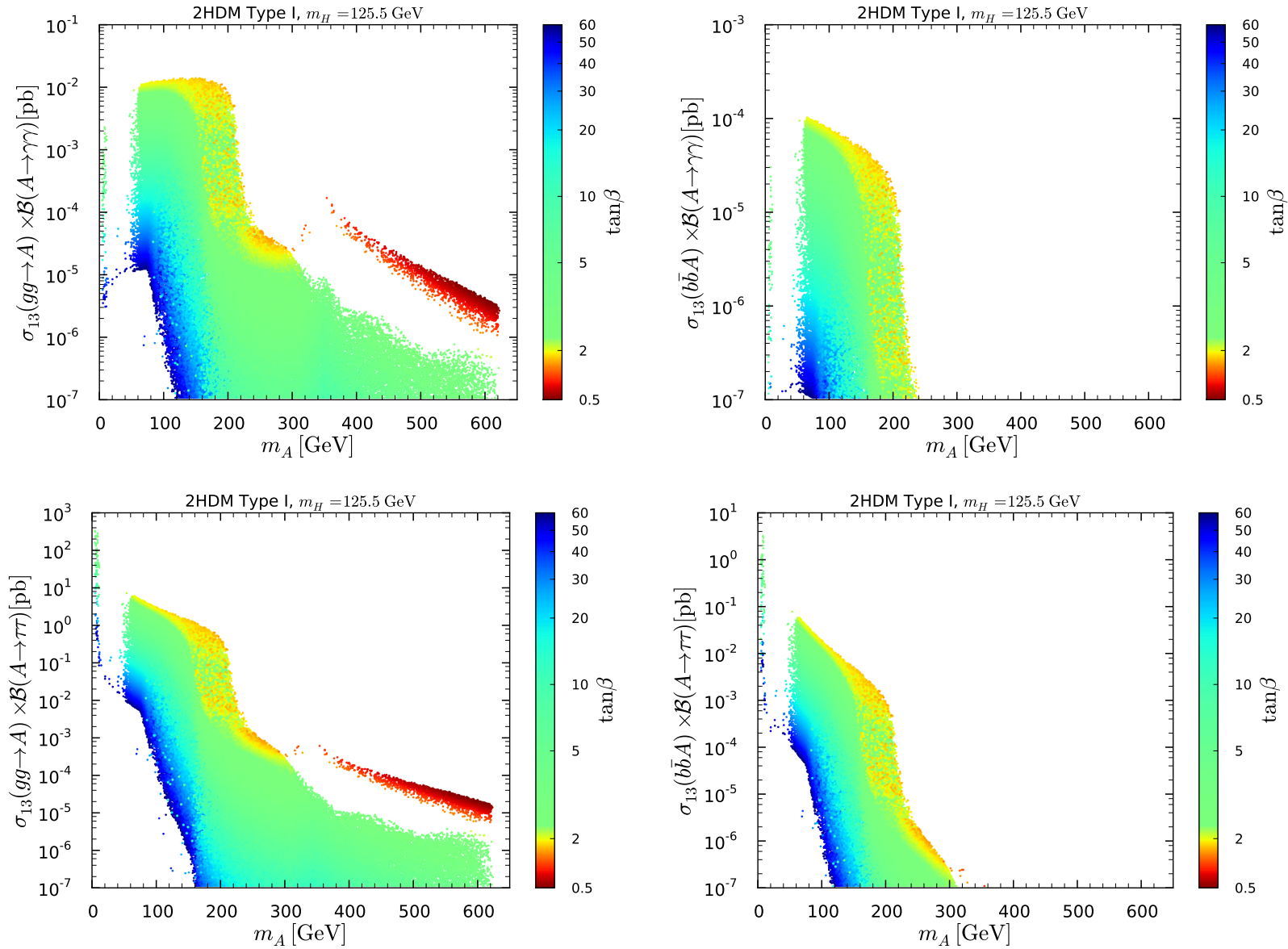
Figure 9: $\sigma \times \mathcal{B}(A \to Y)$ for $Y = \gamma\gamma$ and $\tau\tau$. Points are ordered from high to low $\tan\beta$.

Look closely for the low-m_A points that are possible in Type I (but not Type II).

Finally, there are the large cross sections for $gg \to A \to Zh$, where $Z \to \ell^+\ell^-$ and $h \to b\bar{b}, \tau\tau$, that are already constraining the $H125$ scenario.
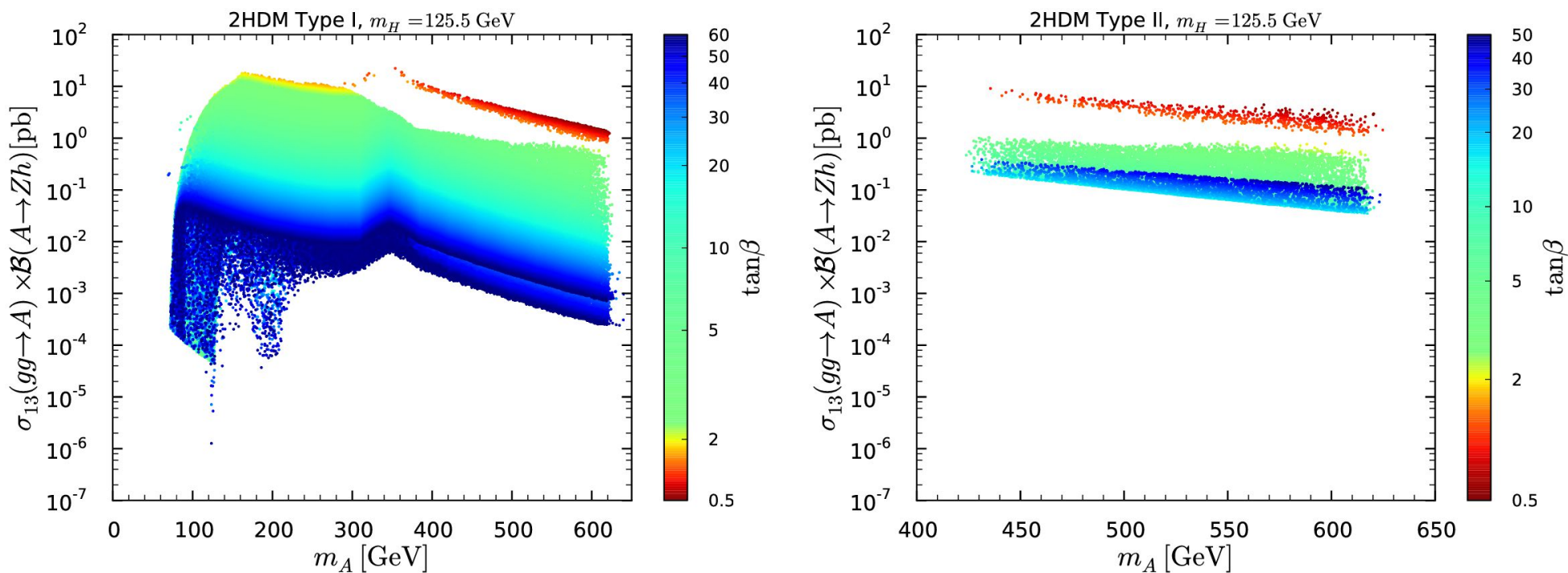
Figure 10: $\sigma(gg \to A) \times \mathcal{B}(A \to Zh)$ in Type I (left) and in Type II (right) at the 13 TeV LHC as functions of m_A with low-to-high $\tan\beta$ color code. Gaps show where current LHC limits have impacted.

Note the well-defined lower limits, which are particularly substantial in the case of Type II. With $\mathcal{B}(Z \to \ell^+\ell^-) \sim 0.06)$ per mode and assuming $\mathcal{B}(h \to \tau\tau) \sim 0.2$ or so for moderate m_h below 125 GeV, we get about 1 fb per mode in the worst Type II case!! This means we can eliminate the Type II $H125$ scenario fairly soon.

750 GeV diphoton signal

- There is a large cross section for $gg \to H \to AA$ over a wide range of m_A, including very low m_A.
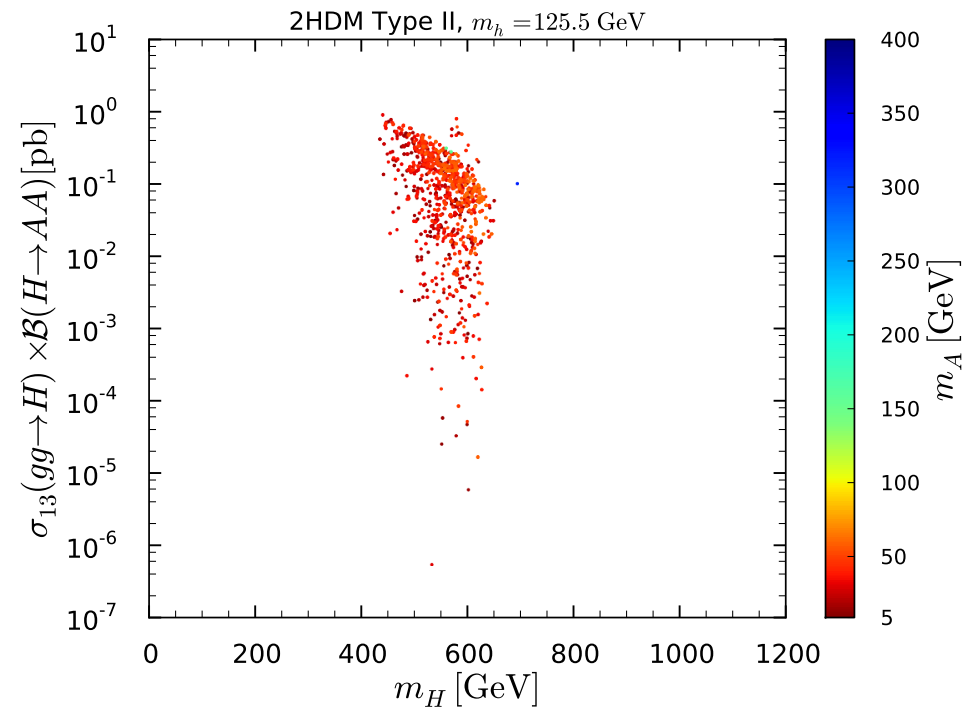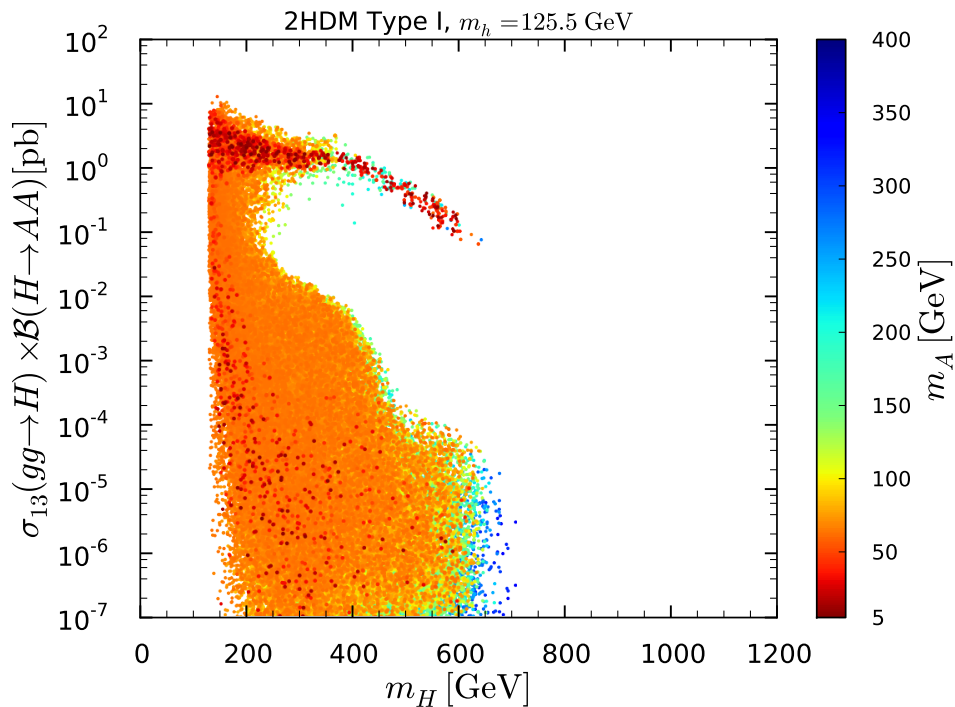
But, the m_H range ends at about $650\,\text{GeV}$. This, upper bound can be expanded somewhat if you relax perturbativity limits on λ_5 2HDM coupling. We restricted $|\lambda_5| < 2\pi$, but if you expand to 4π then no problem.

2HDM Type I, $m_h = 125.5$ GeV

2HDM Type II, $m_h = 125.5$ GeV
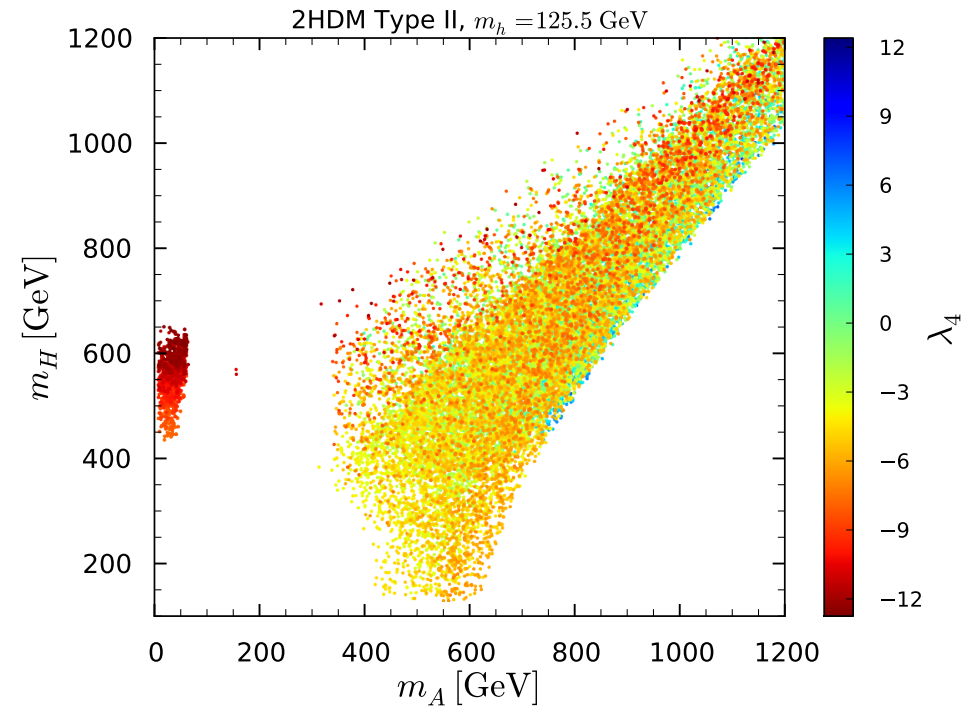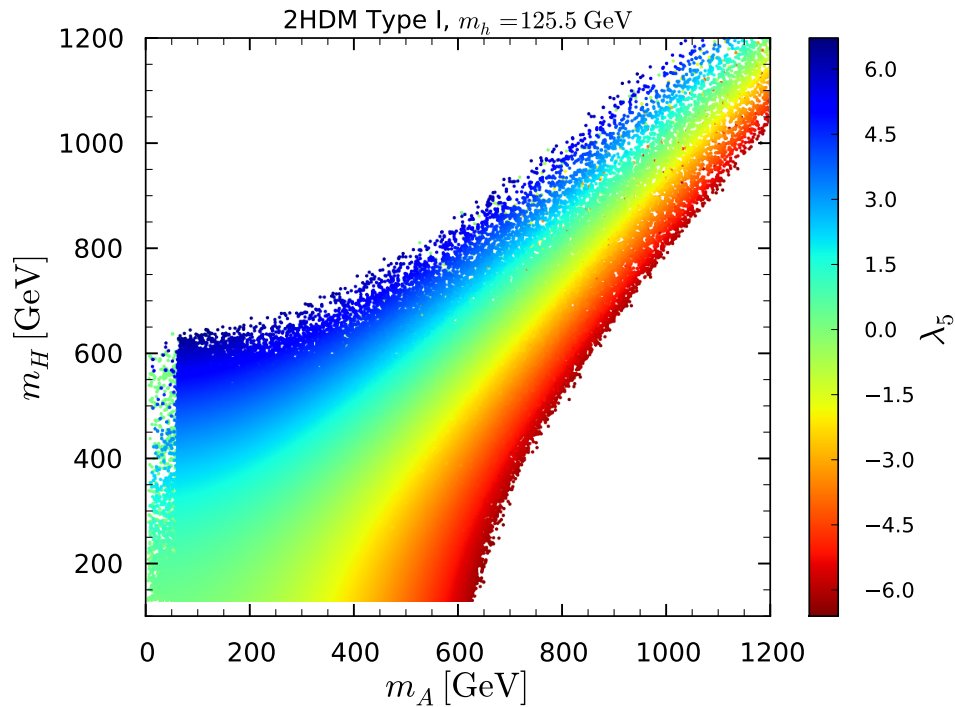
If so, then very easy to get $10\ \mathrm{fb} - 100\ \mathrm{fb}$ cross section for $gg \to H \to AA$ at very small m_A. Then if $A \to \gamma\gamma$ (e.g. it acts like a π^0 or η) then can explain the di-photon signal.

Must be careful about displaced "A" vertices, ...

Higgs Dark Matter Models

1. "Extending two-Higgs-doublet models by a singlet scalar field - the Case for Dark Matter", Aleksandra Drozd, Bohdan Grzadkowski, John F. Gunion, Yun Jiang, arXiv:1408.2106.

2. "Isospin-violating dark-matter-nucleon scattering via 2-Higgs-doublet-model portals", Aleksandra Drozd, Bohdan Grzadkowski, John F. Gunion, Yun Jiang, arXiv:1510.07053

- Suppose there is no SUSY or similar.

  Where can dark matter come from?

- Expanded Higgs sector

  Add a singlet Higgs field that is stable because of an extra Z_2 symmetry that forbids it from having couplings to $f\overline{f}$ and from mixing with the Higgs-doublet field(s) required for standard EWSB.

  An example is starting from the 2HDM and adding a singlet S. After imposing symmetries one ends up with a Higgs potential of the form:

$$V(H_1, H_2, S) = V_{\text{2HDM}} + \frac{1}{2}m_0^2 S^2 + \frac{1}{4!}\lambda_S S^4 + \kappa_1 S^2(H_1^\dagger H_1) + \kappa_2 S^2(H_2^\dagger H_2) \quad (1)$$

Symmetry forbids any linear terms in S. The Higgs portal couplings are the κ_1 and κ_2 terms that induce Higgs-SS couplings when $\langle H_1 \rangle, \langle H_2 \rangle \neq 0$.
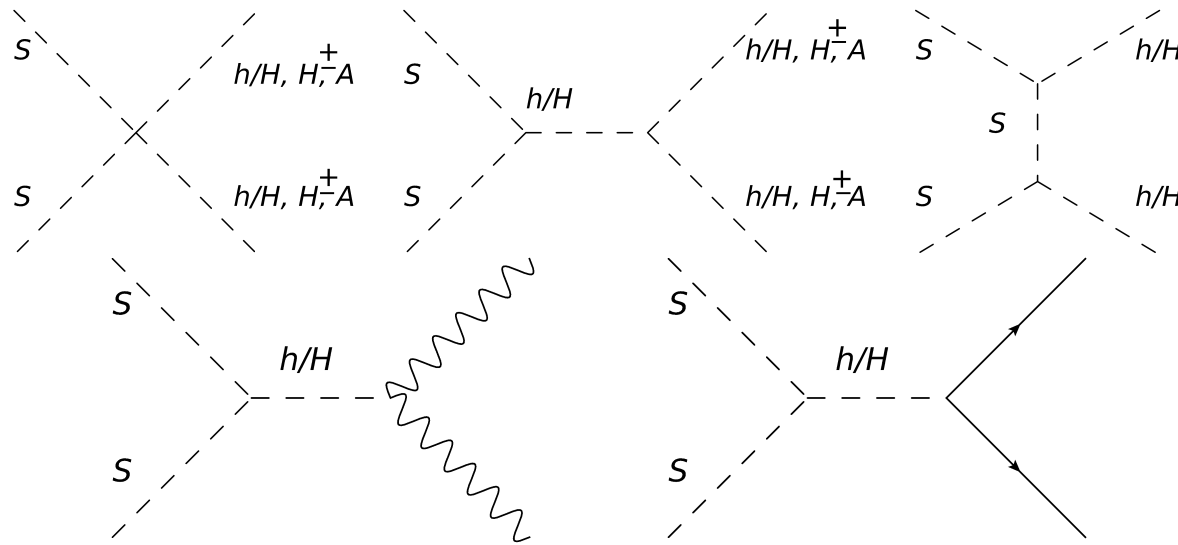
Figure 11: Singlet anihillation diagrams relevant for the relic density calculation.

Singlets are made and annihilate in the early universe by Higgs-related diagrams.

Identifying h of 2HDM sector with the 125 GeV state, one can retain good Higgs fits and get perfectly reasonable dark matter scenarios with $\Omega h^2 \sim 0.11$ and obeying all limits.
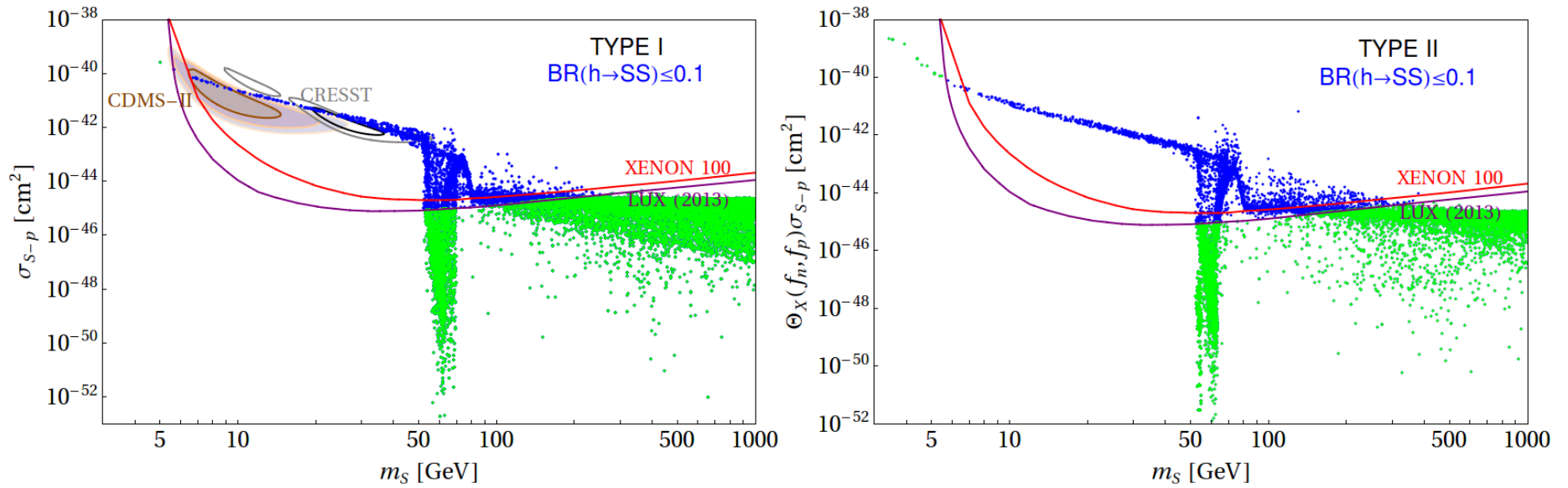
Figure 12: Cross section for DM - proton scattering for the Type I and Type II] models with $\Omega h^2 \sim 0.11$. All points shown satisfy the full set of preLUX constraints, including $\mathcal{B}(h \to SS) < 0.1$, while the green points satisfy in addition the LUX limits. Plots do not include the very fine-tuned 2HDM parameter points with $f_n/f_p \sim -0.7$.

We see that identifying the S with dark matter fails in the $m_S < 125\,\text{GeV}/2$ region because of the need to have very small hSS coupling to keep $\mathcal{B}(h \to SS) < 0.1$ so as to preserve the Higgs fits.

This can be fixed by going to a very special point in 2HDM parameter space: $\tan\beta \sim 1$ and $\alpha \sim -\pi/4$, for which $f_n/f_p \sim -0.7$ at which value the LUX constraints are greatly weakened.

It is also possible to have a similar story in the $H125$ 2HDM scenario.

Conclusions

- The Higgs responsible for EWSB has emerged and is really very SM-like.

  Is it SM-like because of decoupling or because of alignment? We hope for the latter!

- Really light Higgs bosons remain a possibility and in the alignment limit can have encouragingly large cross sections, at least in the 2HDM models.

- We are slowly chipping away at the possibilities for light Higgs bosons that could be present if the 125 GeV state is SM-like because of alignment as opposed to decoupling.

  We must continue to push hard to improve limits/sensitivity to additional Higgs bosons.

- Higgs could be everything, even providing the dark matter.

  This is much easier/less-constrained in the 2HDM + Singlet context than in the SM + Singlet context because either h or H can be the SM-like Higgs at 125 GeV while the other, H or h, respectively, can mediate dark matter annihilation.

- If the 2HDM explanations of the 750 GeV di-photon signal are correct, then we are in for some very exciting times, including heavy vector-like quarks and still more Higgs states.

Radion Model for the Di-photon Signal at 750 GeV: arXiv:1512.05771

Collaborators: Aqeel Ahmed (NCP, Islamabad & Warsaw U.), Barry M. Dillon (Sussex U.),

Bohdan Grzadkowski (Warsaw U.), John F. Gunion (UC, Davis), Yun Jiang (Bohr Inst.).

Jack Gunion
U.C. Davis

CERN, March 22, 2016

The existence of a SM-like Higgs constrains all directions of exploration.

Motivational Issues

- There is a rather SM-like Higgs boson at $m_h = 125$ GeV.

- There is no sign of supersymmetry.

- There is an increasingly convincing excess of di-photon events at $m_{\gamma\gamma} \sim 750$ GeV.

- Maybe it is time to look at alternative models in which there is **no hierarchy problem** and the two observed states are present with the observed cross sections and characeristics.

The Randall Sundrum two-brane model fits the bill. In this model one places the SM, including its Higgs sector, into the context of a 5th (extra) dimension.
Two options:

1. The 750 GeV state is the first excited KK mode of the graviton with mass m_1^{KK}.

2. The 750 GeV state is mainly (but not entirely) the radion, ϕ, of the model, where the radion is the quantum fluctuation associated with the separation of the two branes.

Two more options: do SM particles propagate in the bulk or are they localized on the IR (TeV) brane?

1. Localize on the brane:

   The gluon (and other SM particles) do not propagate in the bulk and hence there are no excited states of the gluon (or any other SM particle). This means that there are no collider bounds on the excited states (KK modes) of the SM particles since they don't exist.
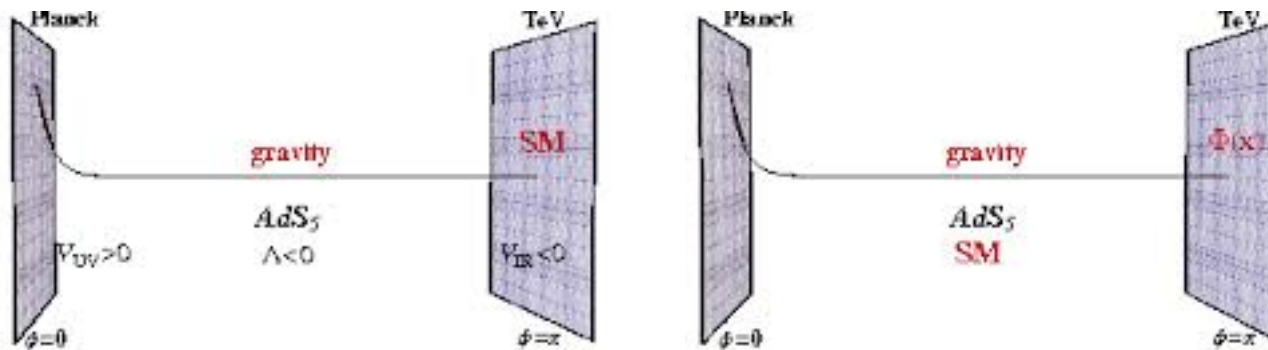

Figure 1: The two RS brane pictures.

2. Allow the gauge bosons and possibly other SM particles to propagate in the bulk.

   The excited state of immediate importance is the first excitation of the gluon with mass m_1^g. In this case, collider data already imply $m_1^g > 3$ TeV.

- Option 1 (KK graviton) has been considered, for example, recently in arXiv:1602.02793.

  - The model has basically one parameter Λ that determines everything once $m_1^{\mathrm{KK}} = 750$ GeV is imposed.
  - $\Lambda \sim 60$ TeV in order to fit the di-photon signal.
  - But, other final states are predicted to have very significant rates. The most worrisome are the $e^+e^-, \mu^+\mu^-$ final states, predictions for which are only very marginally consistent with existing 8 TeV limits (and only at 95% CL). Predictions for these final states at 13 TeV will be easily excluded as Run2 continues.

- Option 2 (Radion) is our choice: arXiv:1512.05771

  - We claim the most (and maybe only) natural interpretation of the 750 GeV state is a radion. It really works very well.
  - In particular, we will see that if the gluon propagates in the bulk then the KK graviton cannot be as light as 750 GeV.

Although dark matter is not present in the simplest incarnation of the RS Higgs-radion approach, it is easily added, for example by adding an extra (stable) singlet to the simplest one-doublet Higgs sector of the model.

Basics of the Model

- RS metric:

$$ds^2 = e^{-2kb_0|y|}\eta_{\mu\nu}dx^\mu dx^\nu - b_0^2 dy^2, \tag{1}$$

  - k is the curvature of the 5D geometry,
  - b_0 is a length parameter for the 5th dimension, and $-1/2 \leq y \leq 1/2$.
  - $\frac{1}{2}kb_0 \sim 35$, for the RS model to constitute a full solution to the hierarchy problem.
  - The fluctuation of the 55-component associated with b_0 is the radion, $\phi_0(x)$. The VEV of ϕ_0 is denoted Λ_ϕ.

- Critical parameter relations:

  - $m_1^{\mathrm{KK}} = x_1^{KK}\frac{k}{M_{\mathrm{Pl}}}\frac{\Lambda_\phi}{\sqrt{6}}$, where $x_1^{KK} = 3.83$ (Note: $x_2^{KK} \sim 7$).
  - $m_1^g = x_1^g\frac{k}{M_{\mathrm{Pl}}}\frac{\Lambda_\phi}{\sqrt{6}}$ $(\sim \frac{k}{M_{\mathrm{Pl}}}\Lambda_\phi)$, where $x_1^g = 2.45$, implying $m_1^{\mathrm{KK}} \simeq 1.55 m_1^g$.
  - Collider data limit of $m_1^g > 3$ TeV, implies $m_1^{\mathrm{KK}} > 4.6$ TeV. This can be avoided at the price of including brane kinetic terms for gauge fields and gravity localized on the "visible" (IR) brane. Without this, only the radion interpretation of the 750 GeV resonance is viable. $\Rightarrow$ The natural choice.

- For the radion interpretation of the $750\,$GeV state it is critical to include a Higgs-gravity coupling, $\xi\mathcal{R}_4 H^\dagger H$ (localized on the IR brane), where

  ξ is a dimensionless parameter and

  $\mathcal{R}_4$ is the four-dimensional (4D) Ricci scalar coming from the induced metric on the IR brane.

  This results in the following 4D effective Lagrangian for the scalar sector,

  $$\mathcal{L}_{\text{eff}} = \frac{1}{2}(\partial_\mu \phi_0)^2 - \frac{1}{2}m_{\phi_0}^2\phi_0^2 - 6\xi\Omega\Box\Omega H^\dagger H + |D_\mu H|^2 - \Omega^4 V(H), \qquad (2)$$

  where ϕ_0 is the (unmixed) radion field and m_{ϕ_0} its bare mass. Above, $\Omega(\phi_0) \equiv 1 - \ell\phi_0/v_0$, where

  $$\ell \equiv \frac{v_0}{\Lambda_\phi} \qquad (3)$$

  with $v_0 = 246\,$GeV and $\Lambda_\phi \equiv \sqrt{6}M_{\text{Pl}}e^{-kb_0/2}$ is the vacuum expectation value (VEV) of the radion field.

  As we will show below, phenomenological constraints make it difficult to accommodate $\Lambda_\phi \lesssim 1.5\,$TeV, implying that ℓ is limited to $\ell \lesssim 1/6$.

- At the quadratic level, the above yields

$$\mathcal{L}_{\text{eff}}^{(2)} = -\frac{1}{2}(1 + 6\xi\ell^2)\phi_0\Box\phi_0 - \frac{1}{2}m_{\phi_0}^2\phi_0^2 + 6\xi\ell h_0\Box\phi_0 - \frac{1}{2}h_0\Box h_0 - \frac{1}{2}m_{h_0}^2 h_0^2, \quad (4)$$

where h_0 is the neutral scalar of the Higgs doublet H, and $m_{h_0} \equiv \sqrt{2\lambda}v_0$ is the bare Higgs mass. In the above Lagrangian, the ξ term that mixes the Higgs and the radion can be removed by rotating the scalar fields into the mass eigenstate basis,

$$\begin{pmatrix} \phi_0 \\ h_0 \end{pmatrix} = \begin{pmatrix} -a & -b \\ c & d \end{pmatrix} \begin{pmatrix} \phi \\ h \end{pmatrix}, \quad (5)$$

where $a = -\cos\theta/Z$, $b = \sin\theta/Z$, $c = \sin\theta + t\cos\theta$ and $d = \cos\theta - t\sin\theta$, with $t \equiv 6\xi\ell/Z$, $Z^2 \equiv 1 + 6\xi\ell^2(1 - 6\xi)$ and

$$\tan 2\theta = \frac{12\xi\ell Z m_{h_0}^2}{m_{\phi_0}^2 - m_{h_0}^2(Z^2 - 36\xi^2\ell^2)}. \quad (6)$$

Given that $\ell \lesssim 1/6$ for the $\Lambda_\phi \gtrsim 1.5$ TeV range of interest and that we will focus on ξ values near the $\xi = 1/6$ conformal limit, it is legitimate to expand Eq. (6) in

powers of ℓ and express the result in terms of the physical mass parameters, m_h and m_ϕ:

$$\tan 2\theta = \frac{12\xi\ell m_{h0}^2}{Z(m_\phi^2 + m_h^2 - 2m_{h0}^2)} \simeq 12\xi\ell \left(\frac{m_h}{m_\phi}\right)^2 \left[1 - 3\xi(1 - 6\xi)\ell^2\right] + \cdots, \quad (7)$$

where the ellipsis stands for terms which are quite small for $m_\phi = 750$ GeV and $\Lambda_\phi \gtrsim 1.5$ TeV. For $\xi = 1/6$ and $\ell \lesssim 1/6$ one obtains $\theta \simeq \ell(m_h/m_\phi)^2 \lesssim (1/6)^3$.

- IMPORTANT: relation between m_1^g (1st gluonic KK excitation), $\langle\phi_0\rangle = \Lambda_\phi$ and the curvature ratio $k/M_{\rm Pl}$:

$$m_1^g = \frac{x_1^g}{\sqrt{6}}\frac{k}{M_{\rm Pl}}\Lambda_\phi \simeq \frac{k}{M_{\rm Pl}}\Lambda_\phi, \quad (8)$$

where $x_1^g \simeq 2.45$ is the 1st zero of an appropriate Bessel function. This relation is depicted in the following figure.
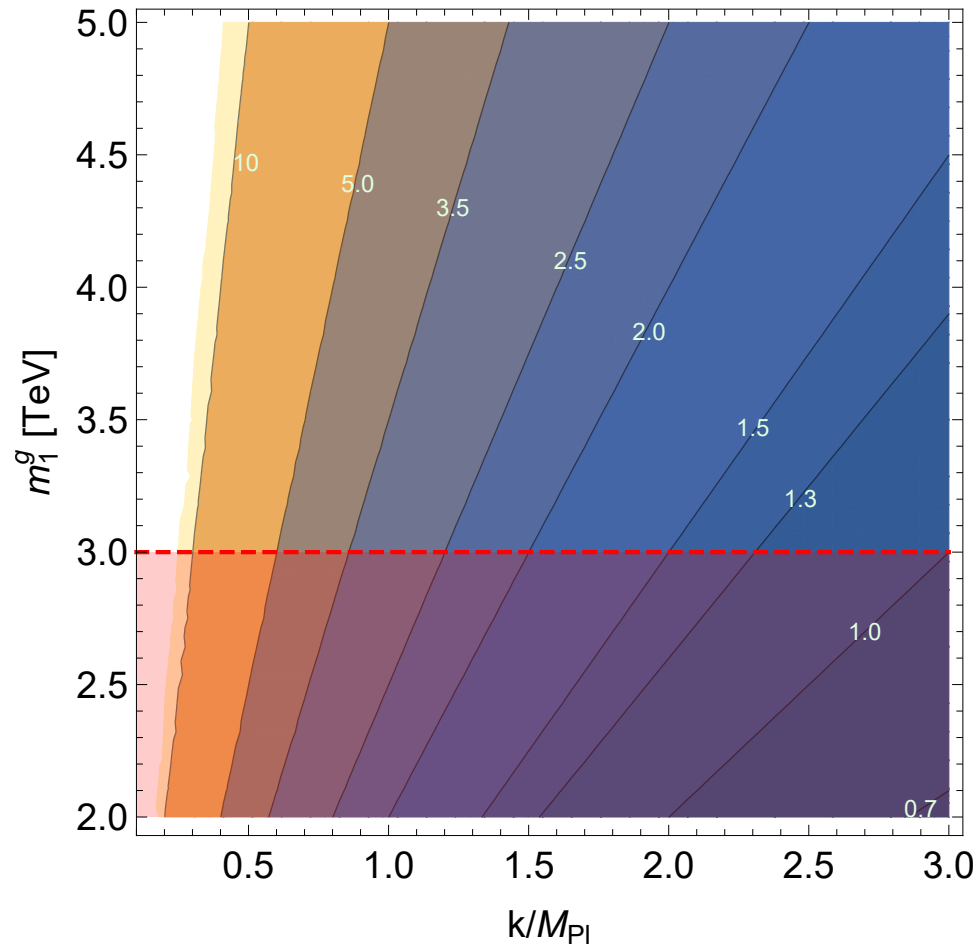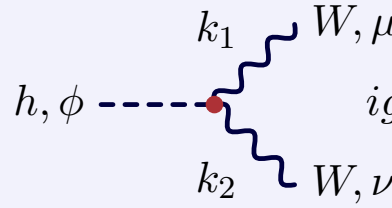
Figure 2: Correlation between m_1^g and k/M_{Pl} for different contours of Λ_ϕ (in TeV). The region below $m_1^g = 3$ TeV (dashed-red line) is excluded by the EWPO and direct collider limits. We will need $\Lambda_\phi \lesssim 2.5$ TeV which implies $k/M_{\mathrm{Pl}} \gtrsim 1$. $\Lambda_\phi = 1.5$ TeV requires $k/M_{\mathrm{Pl}} = 2$ (3) for $m_1^g = 3$ TeV (5 TeV). Originally, k/M_{Pl} values < 1 seemed best motivated; however, more recently k/M_{Pl} values > 1 are deemed equally plausible, with k/M_{Pl} as large as 3 possible without invoking quantum gravity related issues.

- **Particle "locations":**
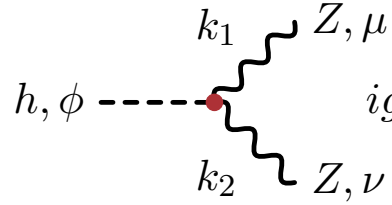
  - The Higgs, t and b will be placed on the IR brane $\Rightarrow$ heavy t natural.
  - We want to place all gauge bosons in the bulk.
    * In the case of the g and γ this is required in order to have enhanced gg and $\gamma\gamma$ couplings.
    * But, if the W and Z are in the bulk, EWPO constraints naively imply $m_1^g > 10$ TeV, which implies too large a value for Λ_ϕ to obtain the observed di-photon cross-section.
    * However, by introducing a local custodial symmetry of $SU(2)_L \times SU(2)_R \times U(1)_X$ (where the $SU(2)_R \times U(1)_X$ fields are broken to $U(1)_Y$ on the UV brane, such that $Y = T_R^3 + X$) then it is possible for m_1^g to have mass as low as $m_1^g \sim 3$ to 5 TeV.
      This is required for the model to have low enough Λ_ϕ, *i.e.* $\Lambda_\phi \lesssim 2.5$ TeV (see Fig. 2) so as to reproduce the observed di-photon cross-section.

- **Couplings:**

  Radion couplings are in Fig. 3. Not shown: the very complicated form of $g_{\phi hh}$.

Diagram 1: h, ϕ → W, μ (k_1) and W, ν (k_2):

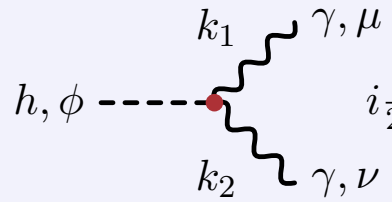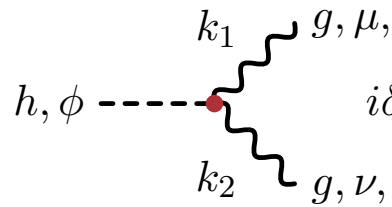$$igm_W\left(g_{h,\phi} - g^r_{h,\phi}\kappa_W\right)\left[\eta^{\mu\nu}\left(1 - 2k_1\cdot k_2 g^W_{h,\phi}\right) + 2k_1^\nu k_2^\mu g^W_{h,\phi}\right]$$

Diagram 2: h, ϕ → Z, μ (k_1) and Z, ν (k_2):

$$ig\frac{m_Z}{c_W}\left(g_{h,\phi} - g^r_{h,\phi}\kappa_Z\right)\left[\eta^{\mu\nu}\left(1 - 2k_1\cdot k_2 g^Z_{h,\phi}\right) + 2k_1^\nu k_2^\mu g^Z_{h,\phi}\right]$$

Diagram 3: h, ϕ → γ, μ (k_1) and γ, ν (k_2):
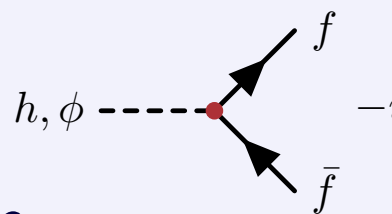
$$i\frac{\alpha}{2\pi v_0}\left[g^r_{h,\phi}\left(b_2 + b_Y + \frac{4\pi}{\alpha k b_0}\right) - g_{h,\phi}\sum_i e_i^2 N_c^i F_i(\tau_i)\right]\left(\eta^{\mu\nu}k_1\cdot k_2 - k_1^\nu k_2^\mu\right)$$

Diagram 4: h, ϕ → g, μ, a (k_1) and g, ν, b (k_2):

$$i\delta^{ab}\frac{\alpha_s}{4\pi v_0}\left[2g^r_{h,\phi}\left(b_3 + \frac{4\pi}{\alpha_s k b_0}\right) - g_{h,\phi}\sum_i F_{1/2}(\tau_i)\right]\left(\eta^{\mu\nu}k_1\cdot k_2 - k_1^\nu k_2^\mu\right)$$

Diagram 5: h, ϕ → f and $\bar{f}$:

$$-i\frac{g}{2}\frac{m_f}{m_W}g_{h,\phi}$$

with $g_h \equiv (d + \ell b)$, $g_\phi \equiv (c + \ell a)$, $g_h^r \equiv \ell b$, $g_\phi^r \equiv \ell a$,

$$\kappa_V \equiv \frac{3m_V^2 k b_0}{2\Lambda_\phi^2(k/M_{\text{Pl}})^2}, \qquad g_{h,\phi}^V \equiv \frac{g^r_{h,\phi}}{g_{h,\phi} - \kappa_V g^r_{h,\phi}}\frac{1}{2m_V^2 k b_0}$$

$$b_2 + b_Y = -11/3, \qquad b_3 = 7$$

Figure 3: Selected radion couplings. The $4\pi/(\alpha_{(s)}k b_0)$ for the $\gamma\gamma$, gg couplings and the κ_V terms and non-SM tensor structures in the WW and ZZ vertices are all due to the vector bosons being present in the bulk.

Notes:

- The coupling of the radion to the trace of the energy momentum tensor implies that the $\phi\gamma\gamma$ and ϕgg couplings have extra "anomalous" contributions with magnitude determined by the respective β functions.
- In addition, the g and γ couplings have $\frac{4\pi}{\alpha_s k b_0}$ and $\frac{4\pi}{\alpha k b_0}$ terms, respectively, added to the anomalous contributions.

  In the $\gamma\gamma$ case, the small size of α implies that this piece dominates the anomaly piece. Indeed, without this extra "bulk" piece the $\gamma\gamma$ signal rate could not be as large as that observed.
- As discussed below, the other pieces (*i.e.* those proportional to g_ϕ) will be small for the choices of $\xi \sim 0.162$ of relevance, where the $t\bar{t}$, $b\bar{b}$ and hh couplings are nearly zero.

  $\Rightarrow$ at $\xi = 0.162$, gg will dominate and $\gamma\gamma$ will be big.

- **Coincident "zeroes".**

1. For the $t\bar{t}$, $b\bar{b}$ the coupling strength is:

$$g_\phi = \ell \left[6\xi \left(\frac{m_h}{m_\phi} \right)^2 + 6\xi - 1 \right] \simeq \ell \left(\frac{37}{6}\xi - 1 \right) \tag{9}$$

One finds $g_\phi = 0$ for $\xi \simeq 0.162162$. **At this point the gg and $\gamma\gamma$ couplings come entirely from the anomalous+bulk contributions**.

2. For the hh coupling one finds:

$$\frac{g_{\phi hh}\Lambda_\phi}{m_\phi^2} = (1 - 6\xi) + \frac{2m_h^2}{m_\phi^2}(1 - 9\xi) - 18\xi\left(\frac{m_h^2}{m_\phi^2}\right)^2 = \frac{19}{18}(1 - 6.17105\xi) \quad (10)$$

Numerically, $g_{\phi hh}$ vanishes for $\xi = 0.162047$, *i.e.* very close to the value for which g_ϕ vanishes.

3. For the $VV = WW, ZZ$ couplings, the external $\eta_V = g_\phi - g_\phi^r \kappa_V$ values are:

$$\eta_V = g_\phi - g_\phi^r \kappa_V \simeq \ell\left[\kappa_V + 6\xi\left(\frac{m_h}{m_\phi}\right)^2 + 6\xi - 1\right], \quad (11)$$

where $\kappa_V = \frac{3kb_0 m_V^2}{2\Lambda_\phi^2(k/M_{\rm Pl})^2} \simeq \frac{105 m_V^2}{m_1^{g2}}$ for $kb_0/2 \sim 35$ using the very good approximation $\Lambda_\phi(k/M_{\rm Pl}) = m_1^g$, see Eq. (8).

For $m_1^g = 3$ TeV, one finds $\kappa_W = 0.0761$ and $\kappa_Z = 0.0981$. As a result, η_V vanishes at $\xi = 0.150, 0.146$ in the W, Z cases, respectively. Of course,

the zeroes shift closer to the $\xi = 0.162$ point for $m_1^g = 5$ TeV, occurring at $\xi = 0.158, 0.157$, respectively.

4. Note that the g_ϕ, $g_{\phi hh}$ and non-κ_V term zeroes all approach the conformal point of $\xi = 1/6$ as $m_h/m_\phi \to 0$.

- **Resulting di-photon signal:**
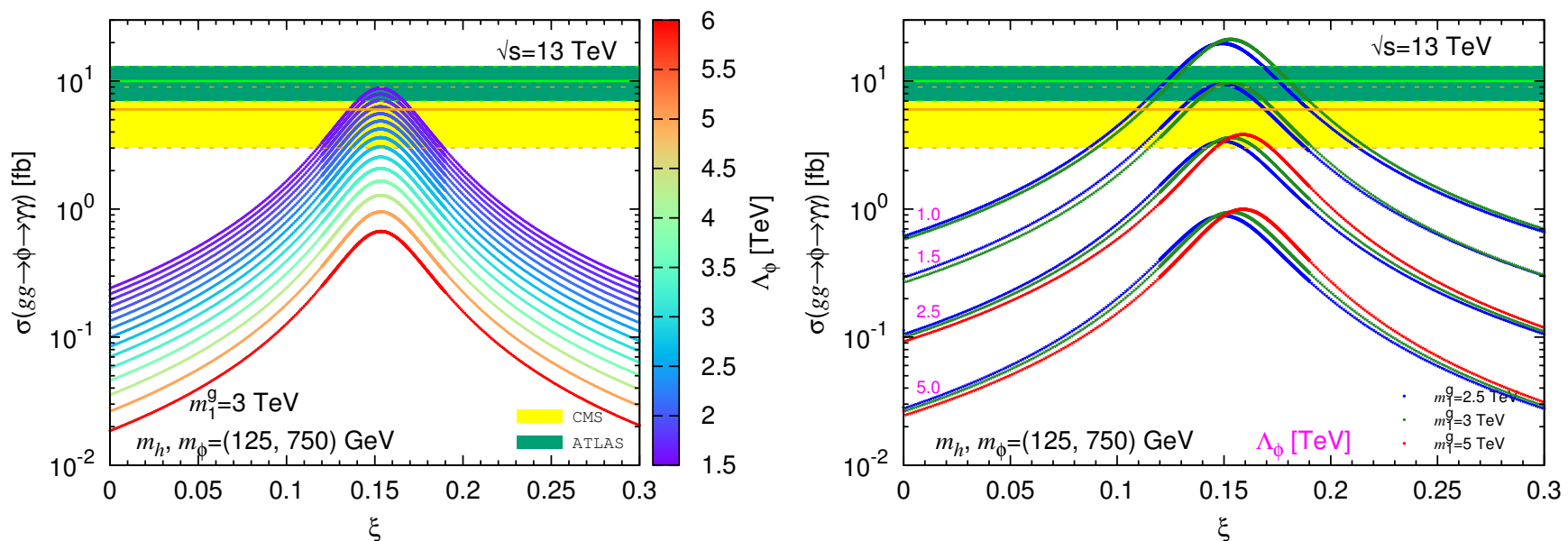
Figure 4: Left: $\sigma(gg \to \phi \to \gamma\gamma)$ as a function of ξ for $m_h = 125$ GeV, $m_\phi = 750$ GeV and $m_1^g = 3$ TeV with different choices of Λ_ϕ as indicated by the coloration. Right: $\sigma(gg \to \phi \to \gamma\gamma)$ for different values of m_1^g and Λ_ϕ. ATLAS and CMS results are the light-green and yellow bands. Need $\Lambda_\phi = 1.5$ TeV to hit "central" values, which, in turn, is only possible if $m_1^g = 3$ TeV given $k/M_{\rm Pl} \leq 3$. Maximal $\gamma\gamma$ rate shifts from $\xi = 0.15$ to $\xi = 0.16$ for $m_1^g = 3$ TeV $\to 5$ TeV.
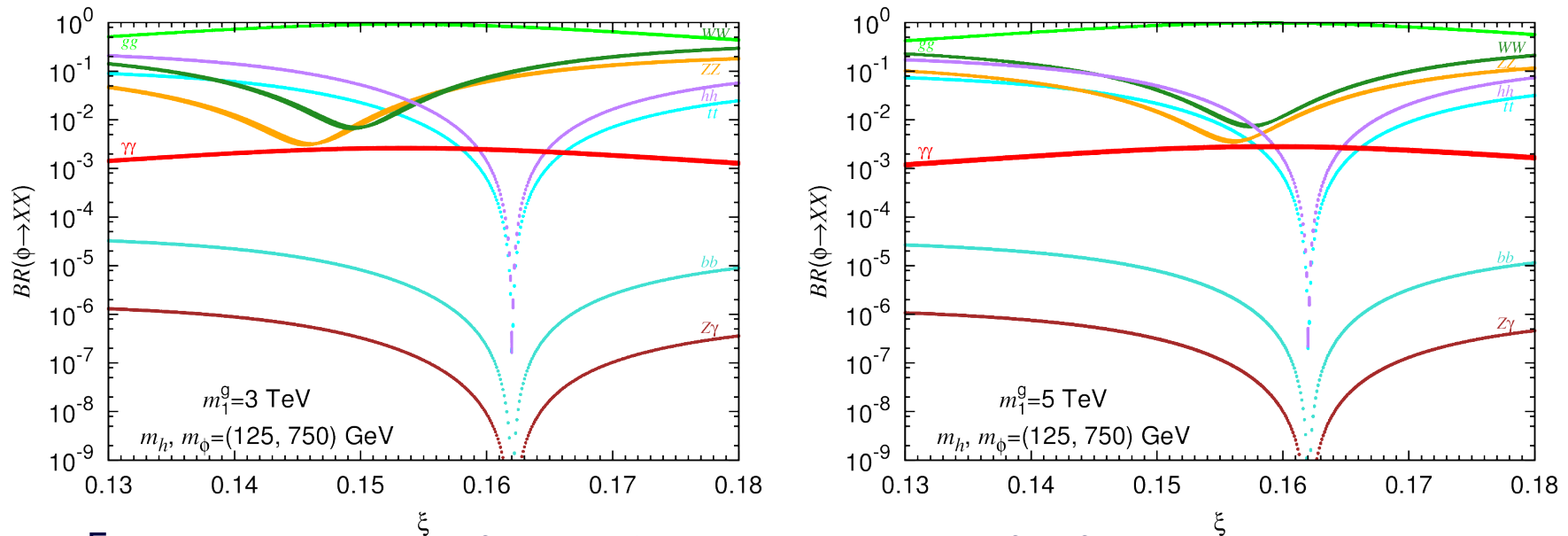
Figure 5: Branching ratios for the ϕ, illustrating the shift of the WW, ZZ minima towards $\xi = 0.162$ with increasing m_1^g. Left: $m_1^g = 3$ TeV. Right: $m_1^g = 5$ TeV. The maximal $\gamma\gamma$ rate is achieved for an intermediate value of ξ between the WW, ZZ minima and the $hh, t\bar{t}, b\bar{b}$ zeroes. Note that the WW, ZZ branching ratios do not vanish because of the extra non-SM tensor structure contributions related the the W, Z residing in the bulk.

A few important points:

– The suppression of all modes aside from $\gamma\gamma$ and gg implies strong production and substantial $\gamma\gamma$ rate, as well as limited constraints from all but the di-jet (gg) final state. More later using some benchmark points.

– **Clearly there are lots of rate correlations that will allow some intimate tests of the model, including determination of Λ_ϕ and m_1^g.**

– In the present one-doublet case, the h is **extremely** SM-like for the ξ values

that give a strong $\gamma\gamma$ signal. But, multi-higgs on the brane is a possibility and then the $h125$ properties can deviate from those of the SM Higgs.

- From the plots of Fig. 6, we see that it is not possible to find a ξ choice such that $\mathrm{BR}(\phi \to \gamma\gamma) > \mathrm{BR}(\phi \to VV)$ for the values of m_1^g that allow Λ_ϕ such as to fit the data. Still, limits on all these final states from the 8 TeV data are consistent with both $m_1^g = 3$ TeV and $m_1^g = 5$ TeV.

- Indeed, we see that there is a rough lower bound on the VV final state branching ratios and so these should appear after sufficient data taking at 13 TeV.

- **The total width of the ϕ is predicted to be well below 1 GeV in this model. This seems to be preferred by CMS but not by ATLAS.**
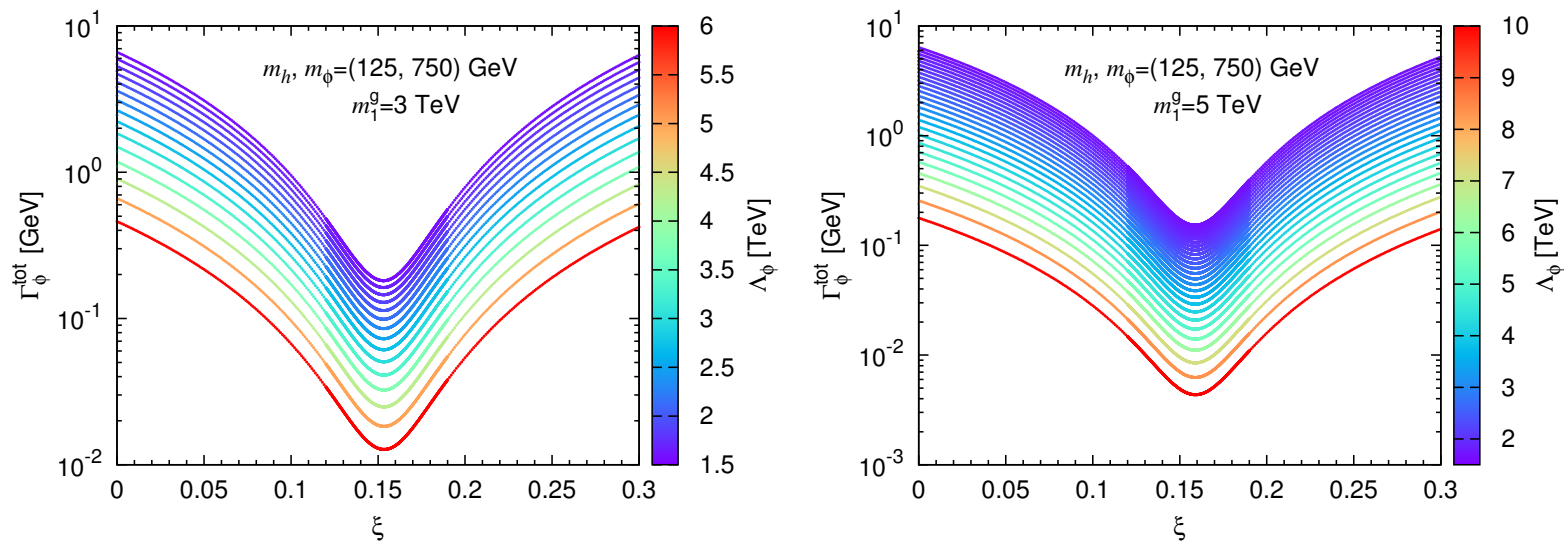
Figure 6: The total width of the radion $\Gamma^{\mathrm{tot}}{}_\phi$, as a function of ξ for $m_h = 125$ GeV, $m_\phi = 750$ GeV, $m_1^g = 3$ TeV (left) or $m_1^g = 5$ TeV (right) with different choices of Λ_ϕ.

– Perhaps most important, the gg final state always has very large branching ratio and should be detectable with future LHC running. Results for $gg \to \phi \to gg$ at 13 TeV are given in Fig. 7.
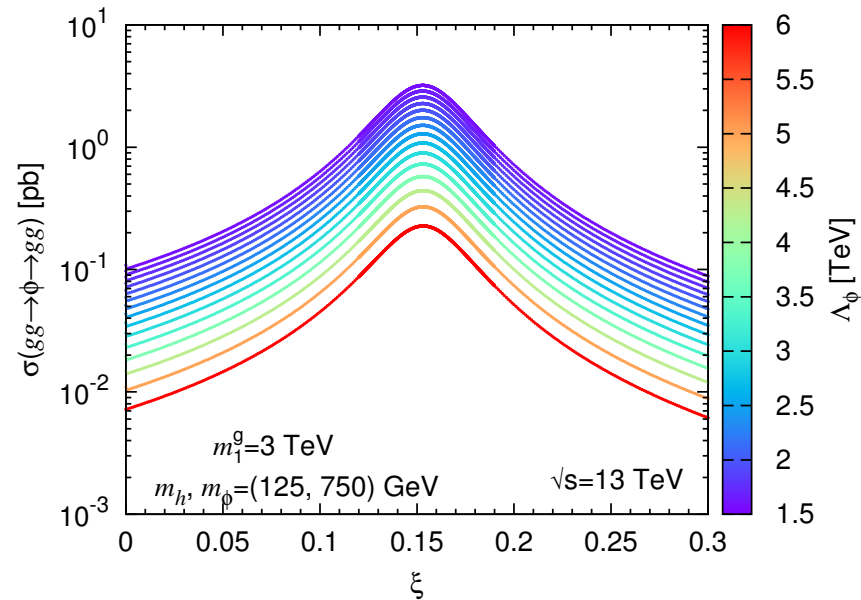
Figure 7: We plot $\sigma(gg \to \phi \to gg)$ as function of ξ for $m_h = 125$ GeV, $m_\phi = 750$ GeV and $m_1^g = 3$ TeV, color-coded by Λ_ϕ.

For ξ values in the region around the peak for which the observed di-photon cross section is well described, one finds $1\text{pb} \lesssim \sigma(\text{gg} \to \phi \to \text{gg}) \lesssim 3$ pb. This is certainly below the $10 \text{ pb}/\mathcal{A}$ bound extrapolated (using factor of 5 luminosity scaling) from the Run 1 limits assuming the same amount of integrated luminosity (20 fb^{-1}). However, for reasonable acceptance at the 13 TeV Run 2, the ATLAS and CMS collaborations should be able to see the gg signal in the di-photon excess region.

Table 1: Ten benchmark points for the Higgs-radion 750 GeV scenario interpretation of the di-photon excess at the LHC. Below Λ_ϕ is calculated for a given m_1^g and $k/M_{\rm Pl}$ according to Eq. (8). The dimensions for the dimensionful quantities are as follows: m_1^g [TeV], Λ_ϕ [TeV], $\Gamma^{\rm tot}_\phi$ [GeV], $\sigma_{gg}^\phi(VV, tt, hh)$ [fb] and σ_{gg}^ϕ (di-jet) [pb]. The cross sections are those at $\sqrt{s} = 13$ TeV.

BMP	m_1^g	ξ	Λ_ϕ	$k/M_{\rm Pl}$	$\mu_{gg}^h(\gamma\gamma)$	$\mu_{gg}^h(ZZ)$	$\mu_{WW}^h(ZZ)$
1	3	0.153	1.5	2	1.013	1.017	0.999
2	5	0.159	1.67	3	1.011	1.015	0.999
3	5	0.159	2.0	2.5	1.008	1.01	0.999
4	5	0.159	2.5	2	1.005	1.006	1.000
5	5	0.159	2.78	1.8	1.004	1.005	1.000
6	3	0.148	1.87	1.6	1.008	1.011	0.999
7	3	0.136	1.58	1.9	1.01	1.014	0.999
8	3	0.153	1.25	2.4	1.019	1.025	0.998
9	3	0.167	1.5	2.0	1.014	1.019	0.998
10	5	0.167	1.67	3.0	1.012	1.015	0.999

BMP	$\Gamma^{\rm tot}_\phi$	$\sigma_{gg}^\phi(\gamma\gamma)$	$\sigma_{gg}^\phi({\rm di-jet})$	$\sigma_{gg}^\phi(ZZ)$	$\sigma_{gg}^\phi(WW)$	$\sigma_{gg}^\phi(Z\gamma)$	$\sigma_{gg}^\phi(t\bar{t})$	$\sigma_{gg}^\phi(hh)$
1	0.201	9.70	3.54	51.2	38.2	7.3×10^{-4}	32.5	75.2
2	0.153	8.37	3.05	12.8	17.6	7.6×10^{-5}	3.38	7.78
3	0.106	5.89	2.12	8.86	12.3	5.3×10^{-5}	2.35	5.42
4	0.068	3.83	1.36	5.65	7.88	3.4×10^{-5}	1.50	3.48
5	0.055	3.12	1.01	4.71	6.55	2.6×10^{-5}	1.14	2.65
6	0.135	6.01	2.18	6.5	14.0	1.2×10^{-3}	51.5	120
7	0.264	6.00	2.22	55.5	200	3.9×10^{-3}	172	398
8	0.288	13.8	5.08	78.4	59.4	1.0×10^{-3}	44.7	103
9	0.256	7.63	2.76	282	392	1.5×10^{-4}	6.50	15.2
10	0.168	7.64	2.77	77.1	122	1.5×10^{-4}	6.52	15.2

We now summarize important aspects of the BMPs.

- Point #1 gives the maximal gg-induced cross section in the $\phi \to \gamma\gamma$ (and, simultaneously, gg) final state for $m_1^g = 3$ TeV when $k/M_{\mathrm{Pl}} \le 2$ is required. As noted above, this corresponds to $\Lambda_\phi = 1.5$ TeV. The maximum occurs at $\xi \sim 0.153$, *i.e.* part way between the minima for the WW, ZZ final state widths and $\xi \simeq 0.162$ where the $t\bar{t}, b\bar{b}, hh$ final state widths vanish. For this point the $\gamma\gamma$ final state has a cross section of order the central ATLAS value. Cross sections in the $hh, ZZ, WW, t\bar{t}$ final states (in that order) range from 75.2 fb down to 32.5 fb, while the gg final state has a cross section of 3.54 pb.

- Points #2 — #5 illustrate results for $m_1^g = 5$ TeV. In this case, the maximal $\gamma\gamma$ cross section occurs at $\xi \sim 0.159$ (since the WW, ZZ cross section dips have moved closer to the $\xi \simeq 0.162$ point at which the $t\bar{t}, b\bar{b}, hh$ cross sections are zero). The different points illustrate results obtained for decreasing k/M_{Pl} values starting from the largest value allowed ($k/M_{\mathrm{Pl}} = 3$). Λ_ϕ ranges from 1.67 TeV up to 2.78 GeV, the latter being the value for which $\sigma(gg \to \phi \to \gamma\gamma)$ is at the lower edge of the CMS observation. Cross sections are ordered according to $WW > ZZ > \gamma\gamma > hh > t\bar{t}$.

The $\gamma\gamma$ cross section for BMP #2 is actually comparable to the case with $m_1^g = 3$ TeV and $k/M_{\mathrm{Pl}} = 2$. This is due to the fact that the Λ_ϕ values

corresponding to points #1 and #2 are very close in size. This is important, since if precision bounds or direct detection bounds push up the limits on m_1^g, this model can still reproduce the properties of the observed di-photon resonance at 750 GeV as observed by ATLAS.

- Comparing points #1 and #4 we observe the effects of increasing m_1^g from 3 to 5 TeV, keeping $k/M_{Pl} = 2$ constant (so that Λ_ϕ increases from 1.5 TeV to 2.5 TeV). As expected, we see a drop in the cross-sections to photons and gluons and in the total width.

- It is important to comment that BMPs #1 — #5 are easily consistent with the LHC 8 TeV data.

- Next, Points #6 and #7 are designed to show the limitation on how large the total width could be when fitting the central $\gamma\gamma$ rate reported by CMS. For the two points considered, we take $m_1^g = 3$ TeV. In these cases, the $\gamma\gamma$ final state cross section is smaller than that for any other final state mode, including the ZZ mode even though in the case of point #6 we have chosen ξ to be close to the ZZ minimum point.

For BMP #6, the total width is increased due to the increased width for the $t\bar{t}$

and hh final states. This is a result of choosing a ξ value that is well below the $\xi = 0.162$ value where the $t\bar{t}$ and hh modes are zero, see Fig. 6.

In the case of BMP #7 we have chosen an even lower value of ξ such that the WW and ZZ modes, as well as the $t\bar{t}$ and hh modes, all have large cross sections. In fact, Point #7 is excluded by existing 8 TeV limits on the hh channel (using a downwards rescaling factor of ~ 5 relative to the 13 TeV value given). This point thus illustrates the fact that one cannot describe the di-photon excess without having a total width well below 1 GeV.

- Point #8 is chosen to have a Λ_ϕ value (1.25 TeV) below our nominal lower limit of 1.5 TeV (which applies if $k/M_{\rm Pl} \leq 2$ and $m_1^g \geq 3$ TeV) in order to illustrate how we can obtain a $\gamma\gamma$ cross section at the upper limit of the ATLAS band. Still higher $\gamma\gamma$ cross sections are, of course, possible by lowering Λ_ϕ further. However, the ZZ final state cross section for this BMP #8 is already on the edge of the 8 TeV ATLAS exclusion limit (using a downwards rescaling factor of ~ 5 relative to the tabulated 13 TeV number).

- Points #9 and #10 are designed to illustrate results for ξ at the exact conformal point, $\xi = 1/6 \simeq 0.167$, with Λ_ϕ chosen so as to give a $\gamma\gamma$ cross section near the center of the ATLAS+CMS band in the cases of $m_1^g = 3$ TeV and 5 TeV,

respectively. The very large WW and ZZ cross sections in the $m_1^g = 3$ TeV case translate to $\sqrt{s} = 8$ TeV cross sections that exceed current limits. At $m_1^g = 5$ TeV, the WW and ZZ cross sections are large, but not in conflict with existing limits, although the ZZ final state prediction for 8 TeV is very close to the ATLAS exclusion limit. Thus, the conformal-limit choice for ξ is viable if m_1^g is large enough and Λ_ϕ is not much above 1.5 TeV.

Of course, these two points illustrate again the limitations on obtaining a large width for the 750 GeV radion state. In these cases we are making a ξ choice well above the minima of the ZZ and WW final state partial widths, but not so far above the zero of the hh partial width ($\xi = 0.162047$). Therefore (unlike for BMP #7 where the hh width is large) here it is the ZZ and WW final state exclusion limits that restrict our ability to get a total width that is more than a fraction of a GeV.

Important final state limits at 8 TeV.

final state	upper bound@8TeV	reference
di-jet	< 2.5 pb	[arXiv:1407.1376, CMS-PAS-EXO-14-005]
$t\bar{t}$	< 300 fb	[arXiv:1309.2030]
hh	< 36 fb	[arXiv:1509.04670]
WW	< 38 fb	[arXiv:1509.00389, arXiv:1504.00936]
ZZ	< 17 fb	[arXiv:1507.05930]
$Z\gamma$	< 4 fb	[arXiv:1407.8150]

Conclusions

- The Higgs responsible for EWSB has emerged and is really very SM-like.

- RS avoids hierarchy problem and so maybe no supersymmetry. RS requires a radion, the quantum fluctation association with brane separation.

- Have we seen the radion at 750 GeV? It is very consistent with what is seen in the $\gamma\gamma$ mode and absence (so far) of other modes if $\Lambda_\phi \lesssim 2.5$ TeV.

- RS scenario can be extended by allowing more complicated Higgs sector on the brane. Thus, there is no reason not to have additional Higgs bosons.

  One can just add to the Higgs sector of the model with impunity so long as the TeV brane multi-higgs model parameters are chosen so that we are in the alignment limit for whatever Higgs boson has mass of 125 GeV.

  Of course, the $g_\phi \sim 0$ limit is needed to prevent dilution of the $\phi \to \gamma\gamma$ signal rate.

  We must continue to push hard to improve limits/sensitivity to additional Higgs bosons.

- Higgs could be everything, even providing the dark matter.

This is much easier/less-constrained in the 2HDM + Singlet context than in the SM + Singlet context because either h or H can be the SM-like Higgs at 125 GeV while the other, H or h, respectively, can mediate dark matter annihilation.